Topology Optimization of the Electrodes in Dielectrophoresis-Based Devices

Abbas Homayouni-Amlashi*, Laure Koebel, Alexis Lefevre, Abdenbi Mohand-Ousaid, and Aude Bolopion

[a]*FEMTO-ST Institute, CNRS, Univ. Bourgogne Franche-Comté, AS2M department, 24 rue Alain Savary, Besançon, 25000, Bourgogne Franche-Comté, France*

Abstract

This paper aims for developing topology optimization methodology to design the shape of electrodes in Dielectrophoresis (DEP)-based devices. The DEP force is due to a non-uniform electric field induced by applied voltages to the electrodes. Shape of the electrodes has the principal effect on the direction and magnitude of the DEP force. In medical therapy microfluidic devices, DEP force is used for cell sorting and cell separation. While the direction and magnitude of the DEP force are desired to be determined and maximized respectively, the magnitude of the electric field should be minimized to avoid damaging cells. Approaching these goals is counter intuitive where the existing electrode designs are basic. Therefore, a detailed finite element model (FEM) is developed for DEP force and electric field to formulate an optimization problem to maximize the DEP force in a particular direction while there is a constraint on electric field's magnitude. Using the developed FEM, explicit formulations for sensitivity analysis are derived to implement a gradient-based topology optimization. The performance of developed methodology is assessed numerically to determine the direction of the DEP force and constraining the electric field and experimentally in a practical case study of particle trapping in a microfluidic channel.

Keywords: Dielectrophoresis, Topology optimization, Sensitivity analysis, Electrode design, Microfluidic Devices

1. Introduction

DEP is a phenomenon that is primarily found by Pohl. et al [1] in which a force is applied on a polarizable particle inside a non-uniform electric field. This force is used to manipulate, control [2, 3] and sort the particles flowing inside a fluid. DEP has application interests in micro-manipulation [4] cell sorting and medical therapy devices and is crucial in drug efficacy evaluation, cancer diagnostics [5] and cell replacement therapy [6]. The magnitude of DEP force depends on the gradient of the electric field which can be produced by the application of AC or DC voltage on a designed electrode. In this case, the magnitude and direction of the DEP force rely on the shape and geometry of the electrode. Therefore, various shapes for the electrodes are proposed including parallel [7], interdigitated [8], castellated [9], quadrupole [10], annular [11], oblique [12], curved [13], etc. A brief review of each of these designs is reported in [14].

Recently, optimization approaches have been used to design more efficient electrodes. The optimization methods include investigative approach on the basic shapes of the electrodes like rectangular, trapezoidal, etc. [15], different placement of rectangular electrodes [16], shape optimization using genetic algorithm [17, 18] and microelectrode discretization [19]. In these optimization approaches, the main drawback is that due to the heavy computational time, large rectangular blocks are employed to discretize the design domain for the electrodes. This will restrict the complexity and diversity of the obtained geometry of the electrodes. Indeed, the discretization of the design domain for the electrodes in these researches is more coarse than the regular discretization in the finite element approach. The study which optimizes the shape of the electrodes based on the finite element discretization is the work done by Yoon et al. [20] in which

Email address: abbas.homayouni@femto-st.fr (Abbas Homayouni-Amlashi*)

the topology optimization methodology is introduced as a potential methodology to optimize the shape of the electrodes. However, in this study, the sensitivity analysis which is a crucial part of the gradient-based topology optimization methodology is not formulated. The lack of sensitivity analysis makes the computation time extremely high for gradient based solvers. In addition, the efficiency of the obtained optimized shape of the electrodes is not investigated experimentally. More importantly, constraining the magnitude of the electric field is not addressed in the optimization formulation of the aforementioned optimization approaches in the literature. Limiting the magnitude of the electric field is hugely important in medical therapy microfluidic devices since a high electric field can kill living cells [21]. To limit the electric field, reduction of input voltage is not an efficient solution since there is a nonlinear relationship between the DEP force and electric field. Producing novel shapes of the electrodes for accurate control of the direction of the DEP force and controlling the magnitude of the electric field can be achieved by topology optimization methodology.

Topology optimization is a form of structural optimization based on finite element discretization which distributes the material inside a design domain in an optimal way while there is no prior knowledge of the final optimal layout. This methodology is an algorithmic approach in which the design domain will evolve to the final optimal layout in a sequence of iterations. Topology optimization methodology is primarily proposed for mechanical compliance problems in which the idea was to minimize the deformation of a mechanical structure [22, 23]. When the methodology is well established in the literature [24], it has been applied to various physics including the thermal and heat transfer [25, 26], fluid dynamics [27], aerodynamics [28], optics [29], piezoelectricity [30, 31, 32], electromagnetic [33], etc. Indeed, the interest in using topology optimization is its ability to produce complex designs where intuitive or trial-error approaches are either impossible or inefficient.

In this paper, the topology optimization methodology in particular the SIMP (Solid Isotropic Material with Penalization) approach has been used to optimize the shape of the electrodes in DEP-based devices. First, a detailed FEM is established to model the electric field and DEP force. The optimization problem is formulated to precisely determine the direction of the DEP force and to put a constraint on the magnitude of the electric field. Due to high resolution of the FEM discretization, the number of optimization variables is very high in topology optimization and hence the gradient-based solvers like Method of Moving Asymptotes (MMA) [34, 35] are generally used to solve the optimization problem. In this case, we need to provide the sensitivity analysis in which the gradient of the objective function with respect to the optimization variables is calculated. Thanks to the developed FEM, explicit formulations for sensitivity analysis are derived for DEP force and electric field using the adjoint method. The sensitivity analysis is performed in a general format so the methodology can be used for different DEP-based applications with minor modifications. COMSOL multiphysics is used to verify the developed FEM and to verify the derived sensitivity analysis, the numerical central difference method is used and the results of sensitivities from both methods are compared and reported.

To investigate the performance of the developed methodology, a numerical investigation is performed to study the efficiency of the methodology in terms of an accurate definition of the DEP force's direction and to reduce the electric field in a desired zone. Moreover, a particular case study has been defined as trapping the randomly distributed particles inside a desired convergence zone in a fluid flowing inside a microdimensional channel. The optimization problem is defined to determine the direction of the DEP force in the desired convergence zone. Two optimized electrodes with two different surface areas are obtained from the developed topology optimization methodology. Then, these two optimized designs are transferred to the COMSOL multiphysics platform for the simulation. The trapping efficiencies of the optimized designs are compared with a U-shape design which has been designed for the same purpose [36] recently. Videos of simulating the particle trapping performances of the designs are added as supplementary materials. In the final step of the research, the optimized designs are fabricated on a fluidic chip and their performance in trapping the beads inside the desired convergence zone is investigated experimentally. The video recordings of experimentation which demonstrate the performance of different designs in terms of particle trapping are provided as supplementary materials.

The paper is organized as follows: Section 2 is devoted to the modeling of the system which starts with the definition of the DEP force and is followed by a detailed FEM which will be used in section 3 for the implementation of topology optimization. In section 3, the SIMP approach is implemented, the optimization problem is formulated and sensitivity analysis is performed. In section 4, the performance of the developed methodology is examined in several numerical case studies to determine the direction of the DEP force and constraining the electric field. In section 5, a case study is defined to assess the performance of the developed methodology for particle trapping inside a microfluidic chip. In section 6, the results of the optimization algorithm written in MATLAB are presented. In section 7, the obtained electrode designs are validated primarily by simulation in the COMSOL multiphysics platform and later by experimental investigation. There will be a discussion on the results and methodology in section 8, and finally, the conclusion of the work is presented. The fabrication process and description of the experimental setup are provided in the appendix.

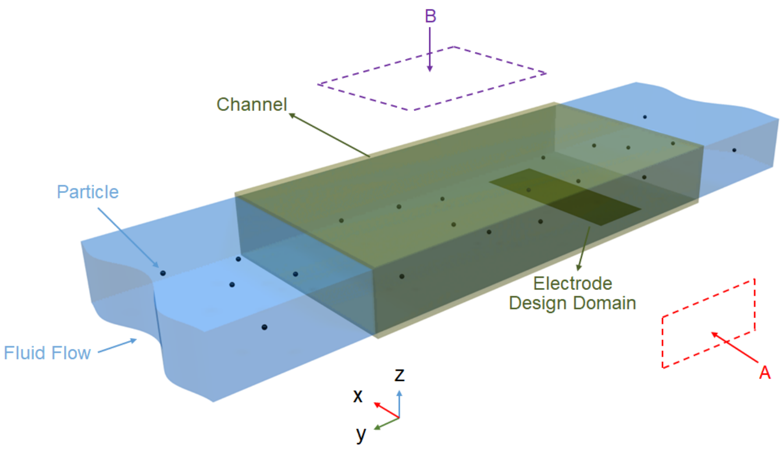

Figure 1: Overview of the fluid containing particles at random positions flowing inside a channel

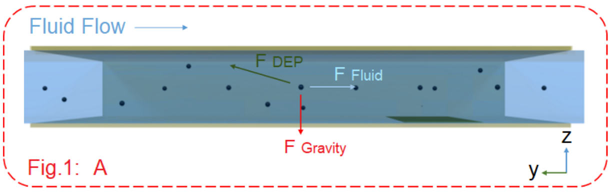

Figure 2: Forces on a particle inside a fluid with non-uniform electric field

2. Modeling

Consider a fluid containing randomly distributed particles flowing inside a channel as it is illustrated in Fig. 1. At the bottom of the channel, there are electrodes with unknown geometry. These electrodes apply DEP forces on the particles inside the fluid by producing a non-uniform electric field. Particles inside the fluid flow are under the application of various forces which are illustrated in Fig. 2. Regarding the introduced physic of interest, several assumptions are considered in modeling process without loss of generality:

- the gravity and fluidic forces are not considered in the physical modeling,
- particles are assumed to be spherical,
- mutual particle interactions are neglected,
- particle interactions with walls of the channel are neglected

First assumption is considered to focus on the DEP force. Second assumption simplifies modeling the DEP force. With third assumption, the study will be done on each particle solely without considering other particles' effects. With these assumptions, the general modeling of DEP force can be represented.

Any particle in a non-uniform electric field will experience an electrostatic force due to Maxwell's stress tensor. For a spherical particle, Maxwell's stress tensor generates a dielectrophoretic (DEP) force on the polarized particle that can be expressed as [37, 38]

$$F_{DEP} = 2\pi\varepsilon_m r^3 Re(f_{CM})\nabla|E|^2 \tag{1}$$

In which r is the radius of the particle, ε_m is the permittivity of the medium (fluid), ∇ is the vector differential operator and E is the electric field,

$$E = -\nabla\Phi \tag{2}$$

where Φ is the potential field. In addition, in equation (1), f_{CM} is the Clausius Mossotti factor that can be calculated as

$$f_{CM} = \frac{\varepsilon_p^* - \varepsilon_m^*}{\varepsilon_p^* + 2\varepsilon_m^*}$$
$$(\varepsilon_p^* = \varepsilon_p - j\frac{\sigma_p}{\omega}, \varepsilon_m^* = \varepsilon_m - j\frac{\sigma_m}{\omega}) \tag{3}$$

ε_p and σ_p are the permittivity and conductivity of the particle. σ_m is the conductivity of the fluid, ω is the frequency of the AC potential and { * } is the sign of a complex number. For the optimization target of this paper, just the real part of the ε is considered [20]. By inspecting the equation (1), it is obvious that the only term that affects the direction and magnitude of DEP force is the square of the electric field's gradient (i.e. $\nabla|E|^2$). This latter can be maximized or minimized by optimizing the shapes of the electrodes. To do so, an area of the channel will be considered as the design domain for the electrodes as it is illustrated in Fig. 3-(a). The modeling in this paper will be in 2D and the effects of the height of the channel are not considered which simplifies the computational burdensome. Although 2D modeling is an approximation considering the inherently three-dimensional nature of the problem, we will show in the simulation and experimental parts that when the height of the channel is sufficiently low the performance of the electrodes follows their 2D modeling. The 2D design domain is separated into two parts of fluid (white) and electrode (black). In addition, an area (Ω) is considered as target area in which the goal is to modify the magnitude and direction of the DEP force and electric field.

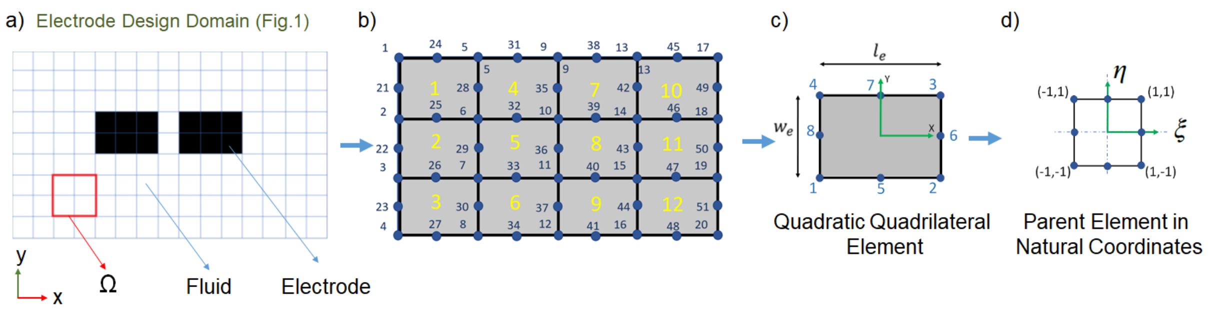

Figure 3: a) Finite element discretization of the design domain with quadratic quadrilateral elements (Ω: Target area) . b) Coarse discretization of design domain. c) Numbering format inside each element. d) Parent element in natural coordinates.

2.1. Finite Element Model

In Fig. 3, the design domain is discretized with finite number of elements. This is a coarse discretization of the design domain for illustrative purposes. From equations (1) and (2), it is obvious that for calculation of DEP force, two times derivative of the potential field is required. As such, the quadratic quadrilateral elements are used to discretize the design domain as it can be seen in Fig. 3-(b and c). These elements have 8 nodes and each node holds a scalar value of potential as degree of freedom. Generally, these elements can have different length (l_e) and width (w_e) [39]. To facilitate the calculations, the parent element in the natural coordinates (ξ, η) is used as it is illustrated in Fig. 3-(d). The connectivity, assembly of elements and numbering format of the nodes and elements are illustrated in panel (b) of Fig. (3). This is helpful for the creation of the global dielectric matrix and final FEM of the system. To support the material presented in this section, more detailed finite element calculation is provided in the appendix. The provided concept will be later used in the modeling of the electric field, DEP force and sensitivity analysis of optimization section.

To build the finite element model, we start by expressing the Gauss law

$$\nabla \cdot (D) = Q \tag{4}$$

where D is the electric displacement vector, and Q is the electric charge. The boundary condition consists of Dirichlet ($\Phi = \Phi_c : \Phi_c$ =constant potential) and Neumann conditions ($n.\nabla\Phi = 0 : n$ = normal vector of the border) [40] which will be explained here after discretizing the design domain. In addition we have the following relation between electric displacement vector (D) and electric field (E),

$$D = \varepsilon E \tag{5}$$

in which ε is the permittivity of the domain that in our paper can be electrode or fluid and it will be determined by the optimization algorithm. Now, by using equations (2, 4 and 5) and considering that the internal virtual work over one element is equal to the work done by the external electric charges over one element [41] the weak form of Gauss law can be written as,

$$\int_{\Omega^e} (\delta E^e)^T D^e d\Omega = -(\delta\phi^e)^T Q^e \tag{6}$$

in which, e is showing that the parameter belongs to the element, ϕ is the elemental potential vector, Q is the charge, δ is the variation sign and Ω^e is the area of one element. By having equation and from the basics of FEM, we can calculate the electric field over an element using the gradient interpolation matrix (B) as follows,

$$E = B\phi \tag{7}$$

Then the elemental dielectric matrix can be calculated as

$$k = \int_{\Omega^e} B^T \varepsilon B d\Omega \tag{8}$$

in which $|J|$ is the determinant of the Jacobean matrix to map the coordinate system from global coordinate to the natural coordinate [42]. The integration over each element can be done using the numerical Gauss quadrature method [42]. Since the elements are quadratic, 3×3 Gauss points can be used to calculate the dielectric matrix with reasonable accuracy. The elemental equilibrium equation can be written as

$$k\phi = Q^e \tag{9}$$

The obtained elemental dielectric matrices for each element should be assembled to obtain the global dielectric matrix. By doing so, the global equilibrium equation in open circuit condition ($Q^e = 0$) can be written as

$$K\Phi = 0 \tag{10}$$

where K and Φ are the global dielectric matrix and vector of potentials respectively. To solve this equation, the potential values of some nodes should be known initially as Dirichlet boundary condition. Through these known values of potentials, the potential values of other nodes can be found with a procedure explained in [43, 44]. For the boundaries of the discretized domain, there is a Neumann boundary condition in which the gradient of potential is zero. The procedures of applying the Dirichlet and Neumann boundary conditions are also explained in [43, 44].

By applying the boundary conditions to the global equilibrium equation (10), the potential field will be obtained and the electric field can be evaluated by using equation (7),

$$\overrightarrow{E} = [B_x\phi]\overrightarrow{i} + \left[B_y\phi\right]\overrightarrow{j} \tag{11}$$

where $\overrightarrow{i}$ and $\overrightarrow{j}$ are the unit vectors in the direction of x and y coordinates system respectively.

For the calculation of DEP force based on equation (1), we need the gradient of the electric field which can be calculated as follows

$$\nabla|E|^2 = \frac{\partial}{\partial x}(E_x^2 + E_y^2)\overrightarrow{i} + \frac{\partial}{\partial y}(E_x^2 + E_y^2)\overrightarrow{j} \tag{12}$$

where in terms of finite element matrices, we have

$$\nabla|E|^2 = \left[2B_x\phi \cdot B_{xx}\phi + 2B_y\phi \cdot B_{yx}\phi\right]\overrightarrow{i} + \left[2B_x\phi \cdot B_{xy}\phi + 2B_y\phi \cdot B_{yy}\phi\right]\overrightarrow{j} \tag{13}$$

In which, the calculation of derivatives of gradient interpolation matrices (i.e. B_{xx}, B_{yy} and B_{xy}) is mentioned in appendix. By using equation (13), the DEP force in equation (1) can be calculated.

After developing the FEM for the electric field and the DEP force, it is possible to enter the optimization phase to design the shape of the electrodes.

3. Optimization

In this section, the goal is to optimize the shape of the electrode to maximize the DEP forces in a desired direction in the target area (Ω) to modify the particle's trajectory inside the fluidic channel. This desired direction can be in any direction based on the application. However, the procedure of deriving the sensitivity analysis remains the same for any other direction. In addition to direction, minimizing the magnitude of electric field is also important since it can damage the living cells. Therefore, the optimization problem should be formulated by definition of the objective function, constraints and optimization variables. These terms will be defined in the following sections.

3.1. Objective Definition

To define the optimization problem in a general format, we can consider a target area (Ω) in the design domain (Fig. (3)-(a)) in which the goal is to maximize or minimize the DEP force in a particular direction and maximize or minimize the magnitude of electric field. Therefore, We have to define cost functions for DEP force and electric field. For DEP force, let's suppose that the goal is to maximize the DEP force in the x direction then the cost function can be defined as

$$\bar{G}_{x-\Omega} = -\int_{\Omega} \frac{\partial}{\partial x}(E_x^2 + E_y^2)d\Omega \tag{14}$$

The cost function in (14) is defined similar to the Ref. [20]. However, in this reference, the method for calculation of this integration which is essential for the sensitivity analysis has not been provided. Here, we use the natural coordinates and the Gauss points which are introduced in the previous sections to calculate the cost functions and to perform the sensitivity analysis in the next section. To calculate the integration (14) over the area of each element, the design domain is already discretized to a finite number of elements. Since the elements are quadratic, 3×3 Gauss points are used for accurate approximation of the integral values. As such, by using the equations (45-13), the integration in equation (14) can be calculated,

$$\bar{G}_{x-\Omega} = \sum_{e}^{\Omega}\sum_{i=1}^{3}\sum_{j=1}^{3} W_i W_j \left[2B_x(\xi_i,\eta_j)\phi B_{x,x}(\xi_i,\eta_j)\phi + 2B_y(\xi_i,\eta_j)\phi B_{y,x}(\xi_i,\eta_j)\phi\right]|\bar{J}| \tag{15}$$

In equation (15), $\nabla|E|^2$ is calculated on each Gauss points (ξ_i and η_j) and the inner summations by Gauss weighting factors W_i and W_j [42, 45], give an scalar value for the integration of $\nabla|E|^2$ over one element (e). Then, the external summation calculates the sum of $\nabla|E|^2$ for all the elements inside the target area. Having a scalar value of $\nabla|E|^2$ for each element is necessary for performing the sensitivity analysis.

To modify the magnitude of the electric field over the target area (Ω), the following integration of the Euclidean norm is introduced here,

$$\bar{E}_{\Omega} = \int_{\Omega} (E_x^2 + E_y^2)d\Omega \tag{16}$$

where $\bar{E}_{\Omega}$ represents the sum of the square of electric field's magnitude over a target area (Ω). By using equation (11) and the numerical Gauss quadrature, we can rewrite the variable $\bar{E}_{\Omega}$ as

$$\bar{E}_{\Omega} = \sum_{e}^{\Omega_A}\sum_{i=1}^{3}\sum_{j=1}^{3} W_i W_j \left[2\phi^T B_x^T(\xi_i,\eta_j)B_x(\xi_i,\eta_j)\phi + 2\phi^T B_y^T(\xi_i,\eta_j)B_y(\xi_i,\eta_j)\phi\right]|\bar{J}| \tag{17}$$

The objective function can be defined as the weighted sum of the $\bar{G}_{x-\Omega}$ and $\bar{G}_{y-\Omega}$ to determine the direction of the DEP force and we can consider $\bar{E}_{\Omega}$ as a constraint. This will be discussed in the formulation of optimization problem.

After establishing the finite element model and defining the objective function, the SIMP topology optimization approach can be developed for the physic of interest.

3.2. SIMP topology optimization

There are several approaches to apply the topology optimization methodology [46]. Among them, the SIMP approach which stands for Solid Isotropic Material with Penalization is more popular due to its efficiency and simplicity of implementation. The core concept of the SIMP topology optimization is the material interpolation function which attributes a continuous variable to each element in the design domain to relax a particular property of the material from a binary value to a continuous one [24]. To better understand the SIMP topology optimization algorithm, the implementation steps will be explained in the coming sections.

3.2.1. *Material interpolation scheme*

To apply the SIMP approach, a material interpolation function is used to attribute a permittivity to each element inside the design domain. The permittivities of elements are relaxed to variate between the permittivity of fluid (ε_{min}) and permittivity of conductive electrode (ε_0) in the sequence of optimization iterations. This steering will form the shape of the electrode after the optimization. The optimization variable is a continuous value between zero and one which will be multiplied to the permittivity of the material. This material interpolation scheme can be interpreted as follows [24, 20]

$$k(\gamma) = (\varepsilon_{min} + \gamma^p(\varepsilon_0 - \varepsilon_{min}))\bar{k}, \quad 0 < \gamma \le 1 \tag{18}$$

In this equation, p is the penalization factor and variable γ is the optimization variable that varies between a very low value to the maximum value of one. The normalized elemental dielectric matrix $\bar{k}$ is defined by factorization of the permittivity from equation (8)

$$\bar{k} = \int_{\Omega^e} B^T B d\Omega \tag{19}$$

The normalized dielectric matrix in equation (19) will be used in the material interpolation equation (18) to form a continuous dielectric matrix. The material interpolation function in equation (18) can also be interpreted by the color spectrum of the design domain where the black color shows the electrode which has the maximum permittivity while the white color shows the fluid with the lowest permittivity. In the iterative sequence of the SIMP optimization algorithm, the elements start from intermediate permittivity (gray elements) and will be steered to the electrode (black elements) or fluid (white elements) permittivities and finally form the shape of the electrode. In this paper, the permittivity of conductive electrode is considered to be 1000 times bigger than the permittivity of fluid.

To steer the optimization variables to zero or one in an optimal way, we need a solution method to update these variables through the iterations. Since we are dealing with a nonlinear optimization problem with high numbers of variables, gradient-based numerical methods will be used as updating algorithm. In this regard, the gradient of the objective function with respect to optimization variables which is known as sensitivity analysis is necessary and will be provided in the next section.

3.2.2. *Sensitivity analysis (DEP force)*

To perform a gradient-based optimization, the sensitivity of the objective function with respect to the permittivity should be calculated. The problem that emerges here is that the gradient of the potential vector with respect to the design variable is not available (i.e. $\frac{\partial \phi}{\partial \gamma}$). To remedy, the adjoint method can be used to avoid the derivation of the potential vector [24, 41]. By using the adjoint method, we augment the equilibrium equation (10) to the objective function (14) using the global adjoint vector Υ which will not change the value of the objective function. In this manner, the integration (15) can be reformulated as follows

$$\bar{G}_{x-\Omega} = \Upsilon^T K \Phi + \sum_{e}^{\Omega} \sum_{i=1}^{3} \sum_{j=1}^{3} W_i W_j \left[2\phi^T B_x^{\mathrm{T}}(\xi_i, \eta_j) B_{x,x}(\xi_i, \eta_j)\phi + 2\phi^T B_y^T(\xi_i, \eta_j) B_{y,x}(\xi_i, \eta_j)\phi \right] |\bar{J}| \tag{20}$$

Now, the sensitivity analysis can be formulated by derivation of the augmented objective function 20 with respect to the optimization variable γ

$$\bar{G}'_{x-\Omega} = \lambda^T k\phi' + \lambda^T k'\phi + \sum_{e}^{\Omega}\sum_{i=1}^{3}\sum_{j=1}^{3} W_i W_j \Big[2\phi^T (B_x^{\mathrm{T}}(\xi_i,\eta_j)B_{x,x}(\xi_i,\eta_j)+$$
$$B_{x,x}^T(\xi_i,\eta_j)B_x(\xi_i,\eta_j))\phi' + 2\phi^T (B_y^T(\xi_i,\eta_j)B_{y,x}(\xi_i,\eta_j) + B_{y,x}^T(\xi_i,\eta_j)B_y(\xi_i,\eta_j))\phi'\Big]|\bar{J}| \tag{21}$$

Here, $'$ is the derivation with respect to optimization variable (i.e. $\frac{\partial}{\partial\gamma}$), λ is the adjoint vector in the elemental level. Moreover, there is a remark about the matrix derivation that has been taken into account for the derivation of sensitivity (21):

Remark: *suppose that we have a scalar value M, which is defined as*

$$M = X^T AX \tag{22}$$

When X is a vector and function of variable z and A is a nonsymmetric square matrix and it is not a function of variable z, then,

$$\frac{\delta M}{\delta z} = X^T(A + A^T)\frac{\delta X}{\delta z} \tag{23}$$

Now to avoid the calculation of ϕ', we have to solve the following adjoint equation

$$\Upsilon^T K + \sum_{e}^{\Omega}\sum_{i=1}^{3}\sum_{j=1}^{3} W_i W_j \Big[2\phi^T (B_x^{\mathrm{T}}(\xi_i,\eta_j)B_{x,x}(\xi_i,\eta_j)+$$
$$B_{x,x}^T(\xi_i,\eta_j)B_x(\xi_i,\eta_j)) + 2\phi^T (B_y^T(\xi_i,\eta_j)B_{y,x}(\xi_i,\eta_j) + B_{y,x}^T(\xi_i,\eta_j)B_y(\xi_i,\eta_j))\Big]|\bar{J}| = 0 \tag{24}$$

The adjoint equation (24) should be solved at the global level. To do so, it can be rewritten in the following format,

$$\Upsilon^T K + \sum_{e}^{\Omega}\phi^T\left[\sum_{i=1}^{3}\sum_{j=1}^{3} W_i W_j \Big[2(B_x^{\mathrm{T}}(\xi_i,\eta_j)B_{x,x}(\xi_i,\eta_j)+\right.$$
$$\left.B_{x,x}^T(\xi_i,\eta_j)B_x(\xi_i,\eta_j)) + 2(B_y^T(\xi_i,\eta_j)B_{y,x}(\xi_i,\eta_j) + B_{y,x}^T(\xi_i,\eta_j)B_y(\xi_i,\eta_j))\Big]\right]|\bar{J}| = 0 \tag{25}$$

Now we can define,

$$\left[\sum_{i=1}^{3}\sum_{j=1}^{3} W_i W_j \Big[(B_x^{\mathrm{T}}(\xi_i,\eta_j)B_{x,x}(\xi_i,\eta_j) + B_{x,x}^T(\xi_i,\eta_j)B_x(\xi_i,\eta_j) + B_y^T(\xi_i,\eta_j)B_{y,x}(\xi_i,\eta_j) + B_{y,x}^T(\xi_i,\eta_j)B_y(\xi_i,\eta_j)\Big]\right] = \boldsymbol{B}_{x,e} \tag{26}$$

The matrix $\boldsymbol{B}_{x,e}$ is a square and symmetric matrix at the elemental level with an equivalent size to the elemental dielectric matrix (k). Therefore, with a similar method, it can be assembled to obtain a global matrix as,

$$\sum_{e}^{\Omega}\boldsymbol{B_{x,e}} = \mathbb{B}_x \tag{27}$$

The assembly procedure of the elemental matrix to obtain the global matrix is explained step by step in the MATLAB codes published for topology optimization [47, 32]. Now by using the global matrix in equation (27), the global adjoint equation can be solved as follows,

$$\Upsilon^T K = \Phi^T \mathbb{B}_x \tag{28}$$

By calculation of the adjoint vector at the global level, it should be dissolved to the elemental level to be used in the sensitivity function. The conversion of the global adjoint vector to the elemental adjoint vector can be done with the help of the connectivity matrix [47] which is used in the assembly procedure of the elemental to global matrices. The detailed procedure can be found in the MATLAB codes published by authors [32]. Finally, the sensitivity equation can be derived as

$$\bar{G}'_{x-\Omega} = \lambda^T k' \phi \tag{29}$$

To obtain the sensitivity, the derivative of the dielectric matrix with respect to the design variable is required as well. By using the material interpolation scheme in equation (18), the derivative of the dielectric matrix can be calculated as

$$k' = p\gamma^{(p-1)}(\varepsilon_0 - \varepsilon_{min})\bar{k} \tag{30}$$

Equations (28 & 29 & 30) form the explicit formulation for the sensitivity analysis of DEP force in the x direction. To validate this explicit formulation, the numerical Central Difference Method (CDM) [48, 49, 50] is used and it is reported in the appendix. The proposed sensitivity analysis is generic. Following the same procedure, one can find a similar formulation for optimizing the DEP force in the y direction in equation (14) or a weighted sum of the objective functions in x and y directions that can accurately define the direction of the DEP force. In addition, the extension to the third dimension is very straightforward. Therefore, the proposed method to derive the sensitivity analysis can be used for topology optimization of the electrodes in various DEP-based applications.

3.2.3. Sensitivity analysis (electric field)

Whether the electric field is considered in the objective function or as a constraint in the optimization formulation, the derivative of electric field with respect to optimization variable should be calculated for gradient-based optimization. To do so, the equation (17) for the magnitude of the electric field can be rewritten as

$$\bar{E}_\Omega = \bar{\Upsilon}^T K \Phi + \sum_{e}^{\Omega}\sum_{i=1}^{3}\sum_{j=1}^{3} W_i W_j \left[2\phi^T B_x^T(\xi_i,\eta_j) B_x(\xi_i,\eta_j)\phi + 2\phi^T B_y^T(\xi_i,\eta_j) B_y(\xi_i,\eta_j)\phi\right] |\bar{J}| \tag{31}$$

As you can see in equation (31), we augmented the equilibrium equation (10) to variable $\bar{E}_\Omega$ once again to avoid the calculation of ϕ'. In this case, $\bar{\Upsilon}$ is the global adjoint vector where ($\bar{}$) is to avoid the confusion with the previous adjoint vectors. Now, the derivative of $\bar{E}_\Omega$ in the elemental format can be calculated as follows

$$\bar{E}'_\Omega = \bar{\lambda}^T k \phi' + \bar{\lambda}^T k' \phi + \sum_{e}^{\Omega}\sum_{i=1}^{3}\sum_{j=1}^{3} W_i W_j \left[4B_x^T(\xi_i,\eta_j) B_x(\xi_i,\eta_j)\phi' + 4B_y^T(\xi_i,\eta_j) B_y(\xi_i,\eta_j)\phi'\right] |\bar{J}| \tag{32}$$

where $\bar{\lambda}$ is the elemental adjoint vector. Then, the following adjoint equation should be solved to avoid the calculation of ϕ'

$$\bar{\Upsilon}^T K = \sum_e^{\Omega}\sum_{i=1}^{3}\sum_{j=1}^{3} W_i W_j \left[4B_x^T(\xi_i,\eta_j)B_x(\xi_i,\eta_j) + 4B_y^T(\xi_i,\eta_j)B_y(\xi_i,\eta_j)\right]|\bar{J}| \tag{33}$$

Equation (33) should be solved at the global level. Therefore, we define,

$$\sum_{i=1}^{3}\sum_{j=1}^{3} W_i W_j \left[4B_x^T(\xi_i,\eta_j)B_x(\xi_i,\eta_j) + 4B_y^T(\xi_i,\eta_j)B_y(\xi_i,\eta_j)\right]|\bar{J}| = \mathbf{B}_{E,e} \tag{34}$$

and matrix $\mathbf{B}_{E,e}$ is a square symmetric matrix at the elemental level with the same dimension as the elemental dielectric matrix and should be assembled to form the global level matrix as follows

$$\sum_e^{\Omega} \boldsymbol{B_{E,e}} = \mathbb{B}_E \tag{35}$$

Now, the adjoint equation (33) can be solved in the global level

$$\Upsilon^T K = \Phi^T \mathbb{B}_E \tag{36}$$

Finally, with finding the adjoint vector, the sensitivity of $\bar{E}_\Omega$ with respect to permittivity can be found by

$$\bar{E}'_\Omega = \bar{\lambda}^T k' \phi \tag{37}$$

Equations (37) and (36) forms the sensitivity analysis for the total magnitude of the electric field. The verification of this sensitivity analysis with central difference method is reported in the appendix.

After defining the sensitivity analysis, the gradient-based numerical solvers can be employed to update the optimization variables. To do so, the optimization problem should be formulated.

3.3. Formulation of optimization

The optimization problem is formulated by the definition of the objective function, constraints and optimization variables. The objective function is the maximization of the DEP force in a desired direction in a desired area. There will be constraints on the surface area or volume with a constant thickness of the electrode and a constraint on the sum of the electric field ($\bar{E}_\Omega$) in the desired area. The optimization variables will be the permittivity of each element in the design domain (γ_i). Now, the optimization problem can be formulated as

$$\begin{aligned} min \quad & \mathbb{J} = W_x\bar{G}_{x-\Omega} + W_y\bar{G}_{y-\Omega} \qquad (W_x + W_y = 1) \\ Subject\ to \quad & V(\gamma) = \sum_{i=1}^{NE}\gamma_i v_i \le V \\ & \bar{E}_\Omega < \bar{E}_d \\ & 0 < \gamma_i \le 1 \end{aligned} \tag{38}$$

In optimization problem (38), the DEP force can be maximized in a particular direction by tuning the weighting factors (W_x) and (W_Y). $\bar{G}_{y-\Omega}$ is the maximization of the DEP force in the y direction in the target area (Ω) (i.e. $\bar{G}_{y-\Omega} = \int_\Omega \frac{\partial}{\partial y}(E_x^2 + E_y^2)d\Omega$). V is the fraction of the total design volume and v_i is the volume of each element. For the SIMP topology optimization, to steer the gray elements to black or white, a constraint on the volume of the material is defined in general [20, 24]. This volume constraint shows the ratio between the volume of the material to the overall volume allowed in the design domain. $\bar{E}_d$ is the maximum allowable sum of electric field magnitudes ($\bar{E}_\Omega$). The constraint on the optimization variables is already defined in equation (18).

With the formulation of the optimization problem, we can build the SIMP topology optimization algorithm to optimize the topology of the electrode.

3.4. Algorithm

The SIMP topology optimization algorithm which has been coded in MATLAB can be written as follows,

Algorithm 1: SIMP topology optimization algorithm for DEP-based applications

```
1  Define the geometrical and material properties, weighting factors, penalization factor, volume
     fraction, filtering and continuation parameters ;
2  Calculate elemental dielectric matrix using equation (8) ;
3  Assemble elemental matrices to build the global dielectric matrix;
4  Define the desired convergence zone ;
5  Define the design and void domains ;
6  Define the boundary conditions (Definition of initial areas of known potentials);
7  Prepare the filtering method [51];
8  Prepare the MMA algorithm [34, 35] (Setting initial values; Move limit = 0.1) ;
9  Initial guess for the permittivity of each element γ_i;
10 while maximum permittivity change > 0.01 or loop number < maximum loop do
11 |  Apply projection and density filter [52, 51];
12 |  Build a new global dielectric matrix based on the updated permittivities;
13 |  Build a new global equilibrium equation based on (10);
14 |  Apply boundary conditions [43, 44];
15 |  Solve the global equilibrium equation (10) and find the system response in terms of potential
   |    field;
16 |  Calculate the electric field and DEP forces;
17 |  Calculate the objective function 𝕁;
18 |  Perform sensitivity analysis based on equations (24-29) and (33-37);
19 |  Applying the builtin MATLAB function "imfilter" to the sensitivities [52];
20 end
21 Update permittivities using sensitivity analysis and MMA algorithm [34, 35];
22 Apply the continuation scheme on the penalty and sharpness factor;
23 Post processing
```

Some steps of the algorithm are explained in previous sections. The other steps will be explained here. In the first line of the algorithm, some parameters should be defined. The parameters and their values are reported in Table 1. In this table, it can be seen that the initial penalization factor is considered to be 2. Indeed, this penalization factor has been proposed by Yoon et al. [20]. However, the penalization in our paper is not constant and it will be increased with the continuation scheme. Based on this continuation scheme, the penalization will start to increase incrementally after iteration number 50. The incremental increase is 0.25 in every 10 iterations and the maximum penalization factor is considered to be 6. The continuation scheme is chosen to facilitate the elimination of intermediate densities (gray elements).

The important step of the algorithm is updating the optimization variables in line 20 of the algorithm. This is where the Method of Moving Asymptotes (MMA) developed by Svanberg [34] is used as the solution method. The implementation code is the second version which is provided in 2007 [35]. In the filtering step (line 19), the goal is to remove the numerical problems like mesh dependencies, checkerboard problem and intermediate densities (gray elements). For the filtering technique, the density filter [24, 47] along with

Heaviside projection suggested by Wang et al. [51] is employed. The complete MATLAB implementation code for this combination of filtering methods is provided by Ferrari et al. [52]. Three parameters in the filtering part should be defined in the first line of the algorithm known as filter radius, threshold and sharpness factor which are reported in Table 1. The continuation scheme is again applied to the sharpness factor. The incremental increase for the sharpness factor is 1 in every 15 iterations which starts after iteration number 50. The combination of the continuation scheme and projection is efficient in terms of steering the elements to fully black and white in the sequence of optimization iterations and removing the gray elements. To stop the iteration loop of the algorithm, the maximum permittivity change between two successful iterations should be less than 0.01 or the maximum number of iterations should be more than 350.

Finally, the last step of the algorithm is post-processing. In this step, the final optimal layout is transferred to the CAD software using the thresholding method proposed by [46] and locating the boundaries of coordinates using the method proposed by [53]. The threshold to steer the remaining gray elements to black and white is considered to be 0.5.

4. Numerical case study

After establishing the SIMP topology optimization based on the detailed finite element modeling, in this section, the efficiency of the developed topology optimization methodology is assessed in several numerical case studies. In these case studies, the efficiency is studied in terms of defining the direction of the DEP force in a target area, maximizing its magnitude and constraining the magnitude of the electric field.

In Fig. 4-(a), the design domain, its initial boundary condition and the target area (Ω) are illustrated. The direction of the DEP force and the magnitude of the electric field should be optimized in this area. The part which is in white will not be changed during optimization. The gray area (design domain) on the other hand will converge to black or white after the implementation of the SIMP topology optimization algorithm. The constraint on the volume fraction is considered to be 0.5. There are boundaries of the design domain that are determined as the initial positions of the electrodes. Indeed, priory known potentials with inverse signs are applied to these boundaries. These initially determined potentials remain unchanged during the optimization. There are other possibilities for the definition of the initial positions of electrodes and even their placement can be a part of the optimization problem. This case is very similar to the optimization of boundary conditions for mechanical compliance problems [24]. However, this is beyond the scope of this paper. The developed algorithm in MATLAB is used to find the optimal shape of the electrodes. The sequence of optimization is not illustrated and only the final results are reported for the sake of brevity. In Fig. 4, different weighting factors (W_x & W_y) are considered for the objective function (38) to determine the desired direction of the DEP force and constraining the magnitude of the electric field. For each case study, two cases of with and without the constraint on $\bar{E}$ are considered. $\bar{E}_d$, is considered to be $\bar{E}/3$ from the case when there is no constraint on $\bar{E}_d$. Optimal layouts for the electrodes and potential fields are plotted for the total design domain while the electric field and DEP forces are plotted inside the target area (Ω) with a color spectrum that shows the magnitude. The parameters related to this numerical study are reported in Table 1.

In case studies (1) and (2) of Fig. 4, the goal is to maximize the DEP force in the x direction while in the case study (2), there is a constraint on $\bar{E}$. The optimized electrode layouts are illustrated in panels (b) and (c). The decrease of the electric field's magnitude in the target area is obvious from panels (n) and (o). In these panels, the color spectrum is set for the same range. The numerical values of $\bar{E}$ and $\bar{E}_d$ are also reported. The algorithm successfully set the DEP force in the x direction as they are illustrated in panels (t) and (u). However, by considering the color spectrum which shows the magnitude of the DEP force, it is obvious that the decrease in the electric field has been done with the cost of decreasing the magnitude of the DEP force.

In cases (3) and (4), the goal is to set the DEP force in the target area in the y direction. The optimal layouts are illustrated in panels (d) and (e). Similar to cases (1) and (2), the algorithm successfully set the DEP force in the Y direction while constraining $\bar{E}$ decreases the DEP force as well. In cases (5) and (6), the goal is to set the DEP force in the diagonal direction. As can be seen in panels (x) and (y), the DEP force is aligned in the diagonal direction.

The numerical study in this section demonstrates the efficiency of the developed methodology in terms

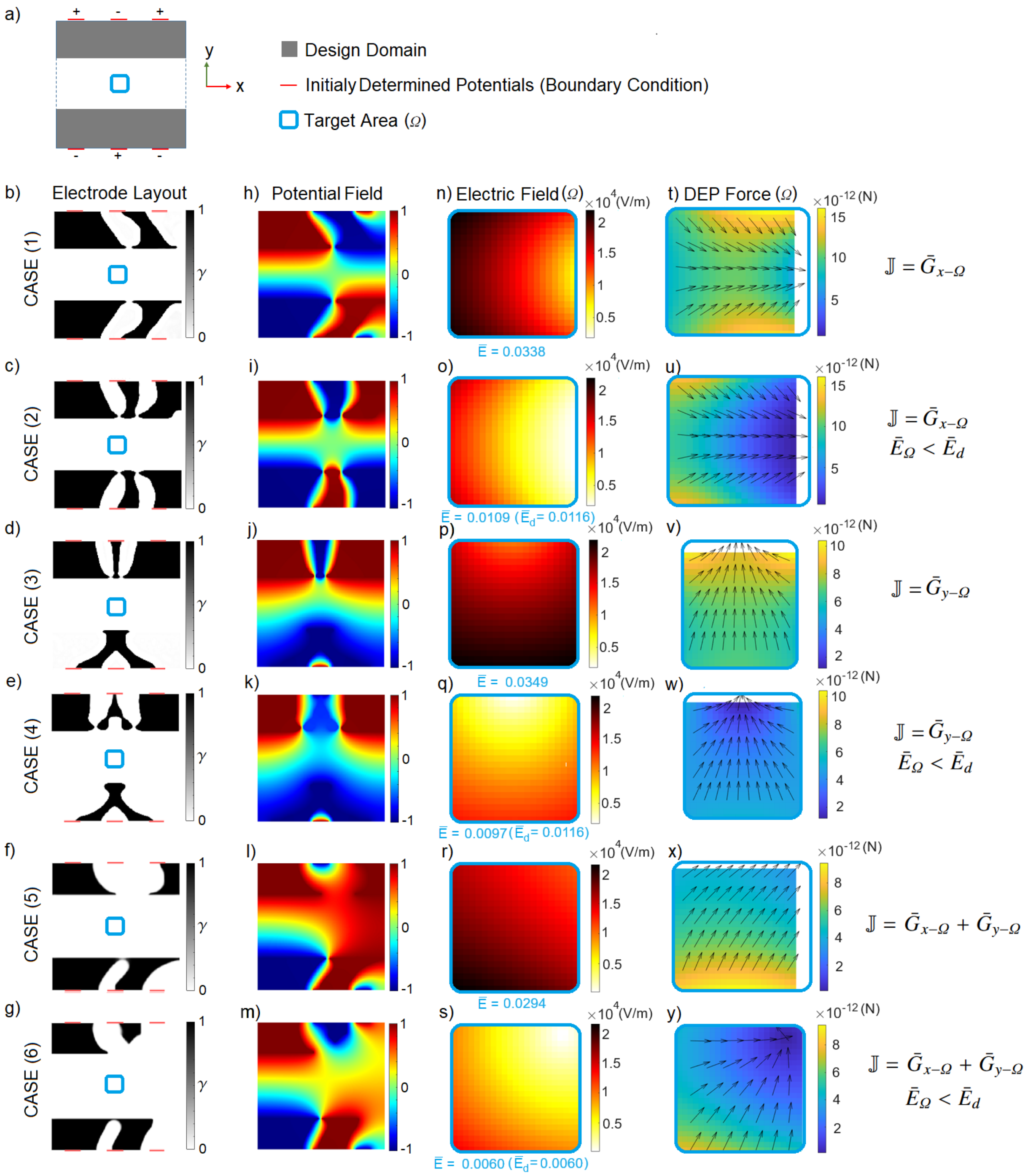

Figure 4: Optimization of electrode layouts to determine the direction of the DEP force and to constrain the electric field. a) Design domain, b-g) Optimal layouts for the electrodes, h-m) Potential field, n-s) Electric field in the target area(Ω), t-y) DEP force in the target area (Ω).

of maximizing the magnitude of the DEP force in a particular direction in a target. Moreover, although there is no control over the local electric field's maximum, constraining the sum of the electric field's magnitude ($\bar{E}$) is successful in terms of reducing its magnitude. In the next section, the efficiency of the developed methodology will be investigated experimentally in a practical case study.

5. Practical case study: Particle trapping in a microfluidic channel

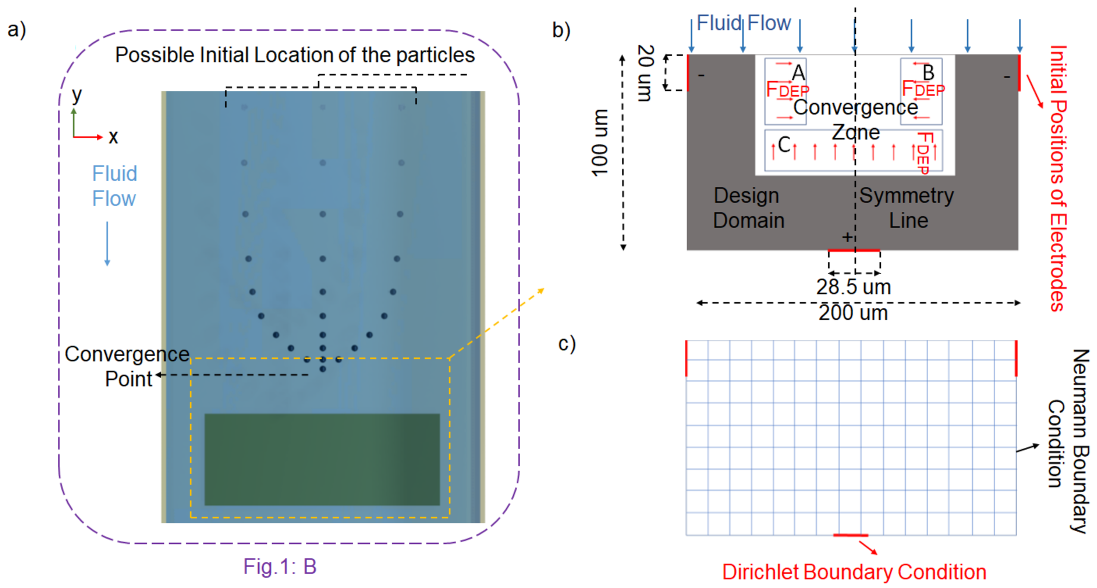

Figure 5: a) Desired trajectory of the particles inside the channel. b) 2 Dimensional representation of the problem c) a coarse discretization of the design domain with imposed boundary conditions.

In this section, the goal is to apply the methodology to a particular case study in which the goal is to trap and stop the particle in a particular region of the channel with the help of DEP force. This case study has particular interests in cell trapping applications [54, 55] to isolate and analyze the tumor cells in cancer studies [56]. The graphical representation of this case study is illustrated in Fig. 5-(a). Based on this figure, if the particles come from certain initial positions in channel, they should converge to a particular region of interest. This desired region which is located in front of the electrode in the middle of the channel will be named in the rest of this paper as the convergence zone. Although some basic geometries were suggested intuitively [14], the idea here is to use topology optimization to find the shape of the electrodes.

As it can be seen in Fig. 5-(b), a gray area is considered as the design domain. The initial position of the electrodes and the sign of applied potentials are defined symmetric to have a symmetrical topology of electrodes and symmetrical DEP forces after the optimization. The current initial positions for the electrode are obtained after a trial-error procedure considering different possibilities.

By considering the goal of trapping the particles, the directions of the desired DEP forces are illustrated in Fig. 5-(b). It is desired to maximize the gradient of the electric field in the y direction in the target area C and in the x direction in the target areas A and B. Keeping into consideration these target areas, the objective function can be defined as the weighted sum of the electric field gradient for each of the areas,

$$\mathbb{J} = W_x(\bar{G}_{x-\Omega_A} + \bar{G}_{x-\Omega_B}) + W_y\bar{G}_{y-\Omega_C} \tag{39}$$

The physical specifications of the channel, electrodes, fluid and particle are mentioned in Table 1. It should be noted that, in this paper, the FEM and the optimization are done in 2D. This means that the behavior of the DEP force and the electric field in the third dimension (z axis) is not considered while in the real application, the behavior of the DEP force in the z direction is also important. Due to the huge fall of the DEP force in the z direction (height of the channel) which will be discussed in the coming sections, the objective function (39) is defined to maximize the DEP force and the minimization of the electric field

Table 1: Parameters

Parameters (Numerical Study)	Values	Parameters (Particle Trapping)	Values
Permittivity of Electrodes (γ)	$78000\gamma_0$	* CZ Length	114.28 μm
Permittivity of Fluid (Water) (γ)	$78\gamma_0$	* CZ Width	40 μm
Penalty Factor (p) (initial)	2	Channel Height	25μm
Volume Fraction	0.5	Channel width	310 μm
Filter Radius	3	Particle Diameter	10 μm
Maximum Iteration Loop	350	Particle Permittivity	$2.56\gamma_0$
Threshold	0.8	Design Domain Length	200 μm
Sharpness factor (Initial)	2	Design Domain Width	100 μm
MMA move	0.1	W_x	0.66
W_E	1.6e-3	W_y	0.33

* CZ : Convergence Zone $\quad$ *γ_0= Permittivity of vacuum

is not considered in the practical case study. Moreover, the polystyrene beads are used as particles and not the living cells. Hence, there were no limits for the electric field.

6. Optimization results for particle trapping

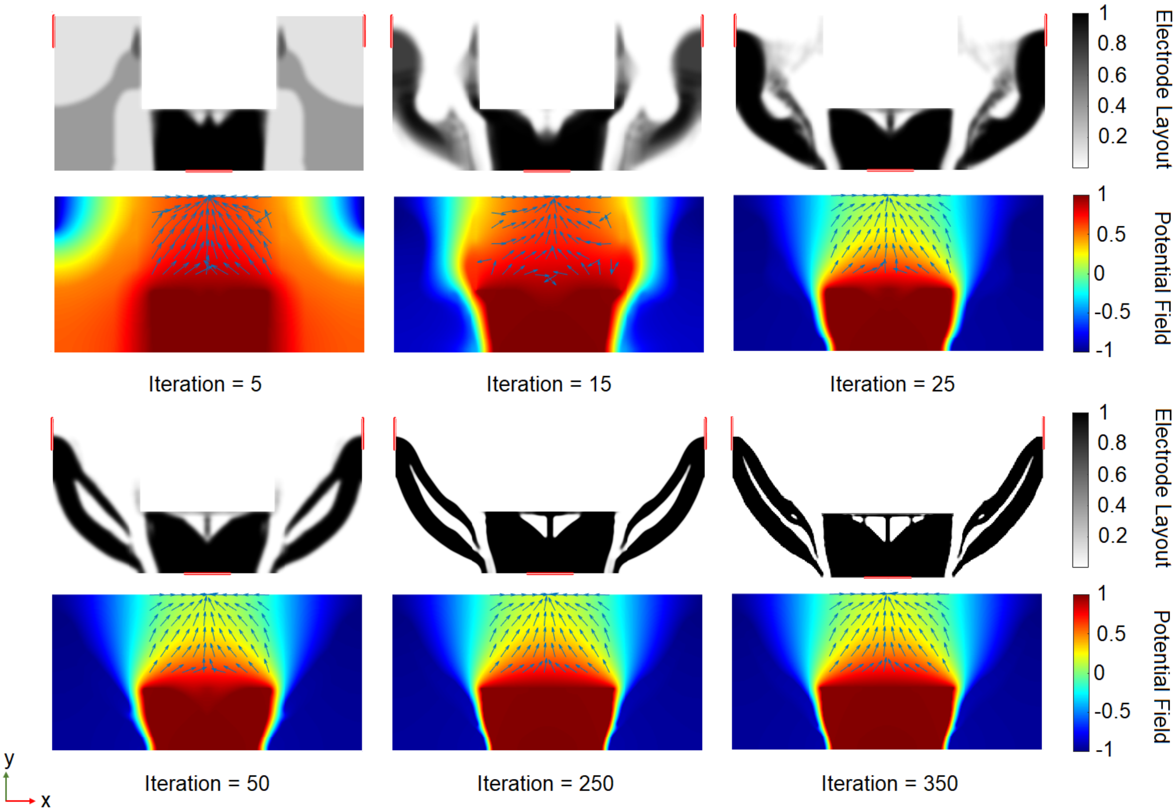

Figure 6: MATLAB topology optimization results for the case of 0.3 volume fraction. Arrows are showing the DEP force direction.

To obtain different optimal shapes of the electrodes, two volume fractions of 0.3 and 0.4 are considered here as constraints which gave the best performance among other possible volume fractions. In Fig. 6 and Fig. 7, the MATLAB topology optimization results for these volume fractions are illustrated. The results are shown for certain iterations. The DEP forces in the desired domain of interest converge to the center and

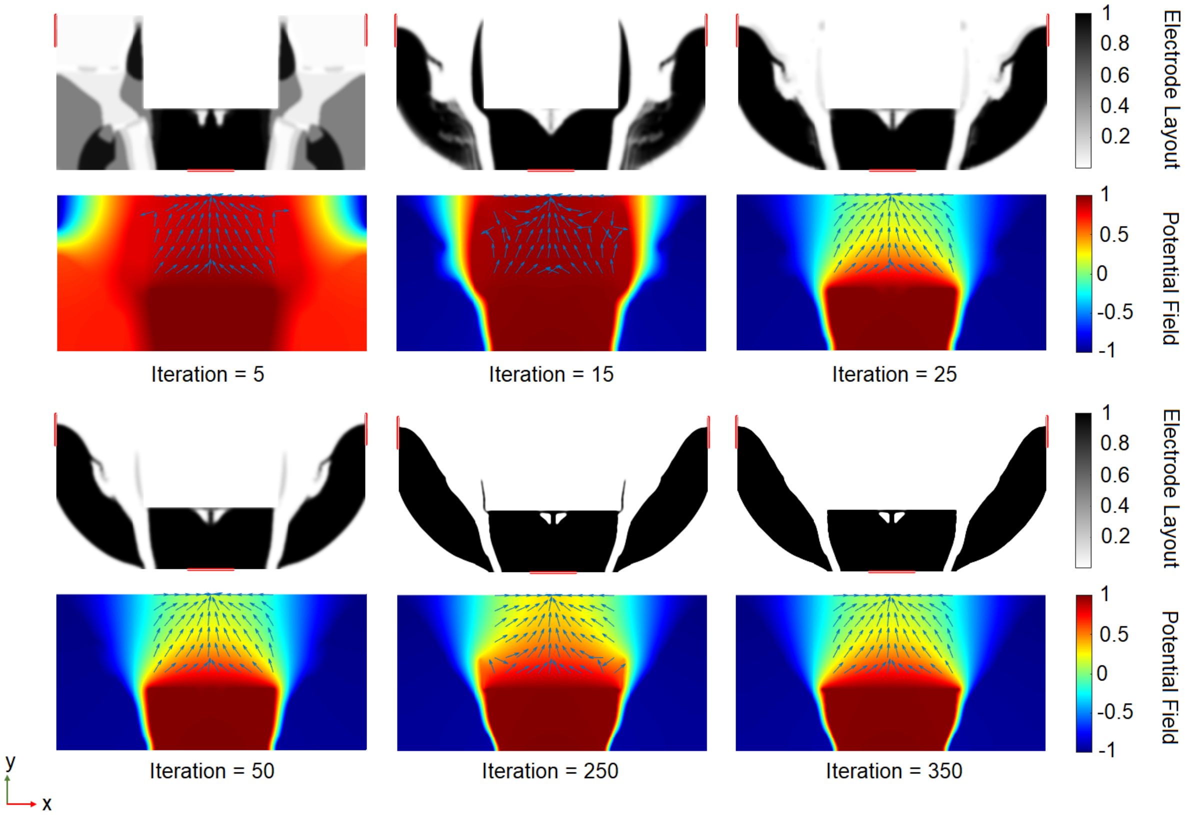

Figure 7: MATLAB topology optimization results for the case of 0.4 volume fraction. Arrows are showing the DEP force direction.

toward the inverse direction of the fluid flow which is in accordance with the defined directions of the DEP forces in Fig. 5-(b). The arrows are normalized to indicate the direction of the DEP force and the amplitude of the DEP forces will be demonstrated later in the simulation part.

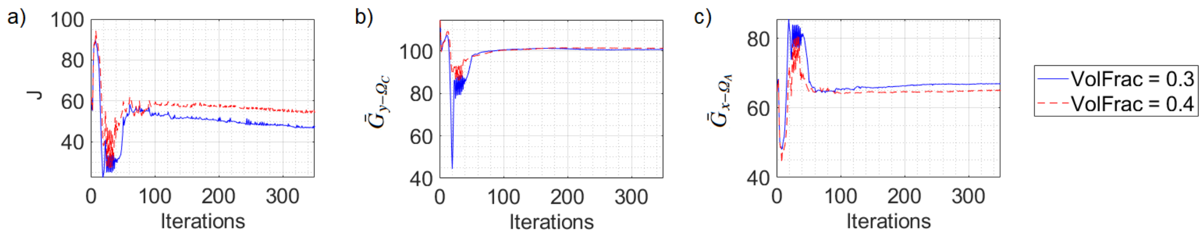

Figure 8: MATLAB optimization data. a) The objective function, b) Square of electric field's gradient in the y direction over the desired area, c) Square of electric field's gradient in the x direction over the desired area.

The numerical data of optimization iterations are reported in Fig. 8. For the two volume fractions, $G_{y-\Omega_C}$ is the same. However, for the volume fraction 0.4, a declination in $G_{x-\Omega}$ can be seen. For this reason, the minimization of the objective function ($\mathbb{J}$) shows better results for the volume fraction 0.3. This result shows that the increase in volume fraction will not necessarily increase the performance of the optimized design in terms of converging the DEP forces toward the center which is expected in the nonconvex optimization problem.

7. Validation of the obtained designs

In this section, the goal is to validate the designs obtained from the MATLAB topology optimization code. As such, this section is divided into two parts of numerical simulation by COMSOL and experimental validation via fabrication of the optimized electrodes. The finite element modeling and optimization in MATLAB have been done with 2D elements. On the other hand, to better understand the actual performance of the optimized design in a real condition, it is necessary to perform the 3D simulation and investigate the efficiency of the optimized design by considering the height of the channel. In order to compare the efficiency of the optimized design with an efficient existing design, a U-shape design inspired from the design which is recently proposed by Punjiya et. al. [36] for cell trapping purposes is also considered during simulation and experiment. It is a 2D electrode that is efficient in trapping particles in the 3D domain of a channel. To make a proper comparison, the modeled U-shape design occupies a similar area to the optimized electrode (0.4) and it is fitted into a similar design domain to the optimized designs. This makes the comparison between the designs fair. Moreover, The chosen design domain gives sufficient freedom to the topology optimization to produce efficient results. To assess the performance of the designs, the potential field and the DEP force in the desired area for trapping the particles are illustrated.

7.1. COMSOL 3D simulation

The channels, convergence zone and electrodes with geometrical dimensions are illustrated in Fig. 9-(a,f,k). In the rest of the panels of Fig. 9, the directions of the DEP force and electric field are illustrated with the help of the streamlines. For the DEP force, the stream lines are just illustrated in the convergence zone for the purpose of better visualization. The color of the streamlines shows the magnitudes with the help of the color bar.

By analyzing the plots in Fig. 9, it can be seen that in the optimized designs the direction of the DEP force is toward the center and opposite to the direction of the flow. This was the predetermined target to trap the particles in the convergence zone. Indeed the stream lines are following the same patterns of the DEP forces in the 2D modeling of Figs. 6 and 7. This proves that the 2D modeling of electrodes is adequately close to their 3D behavior. The only influential factor is the height of the channel which will be discussed later. The same behavior of the DEP force can be seen for the U-shape design but the important point is that we placed the convergence in such a way that it overlaps with the electrode surface. Indeed, the U-shape design produces the maximum amount of DEP force on the face of the electrode while the optimized designs are still capable of producing a satisfactory amount of DEP force in the convergence zone far from the electrode surface. This point can be seen in the panels (e-j-o) of Fig. 9. The amount of electric field for the optimized designs in the convergence zone is less than the U-shape in its convergence zone. By analyzing the DEP force for the U-shape in the z direction, it is obvious that the U-shape pushes the particles to the bottom of the channel while the optimized designs push the particles toward the top of the channel. In this regard, the U-shape is superior to the optimized designs since the DEP force is stronger close to the surface of the electrodes. This is because, in the 2D optimization, the behavior of the DEP force is not considered in the Z direction.

To better understand the behavior of DEP force in the direction of the channel's height, the DEP forces are plotted for certain points in Fig. 10. In this figure, two series of points in the direction of the channel's height are considered in two different positions as can be seen in panel (d) of the figure. The first series of points which are marked with blue color is in the center of the channel in front of the electrode. Another series of points which are marked by red color is a bit far from the center and close to the wall of the desired convergence zone. In panels (a) to (c) of Fig. 10, the magnitude of the DEP forces in 3 directions for all the points for the 3 different designs are depicted. For all the directions, the drop in the magnitude of all DEP forces can be seen by going far from the electrode to the top of the channel. Just the DEP force in the z direction has a peak in the 10 μm and then it drops. The most important plot is the DEP forces in the direction of x which are reported in plot (b). In this plot, the magnitudes of the forces at the side points (red color) drop with the channel's height. This means that, as much as we go far from the electrodes, the convergence performance of the electrodes decays. Since the dimension of the particle is 10 μm, we considered the height of the channel to be 25 μm. Less than this height may not be interesting for the DEP

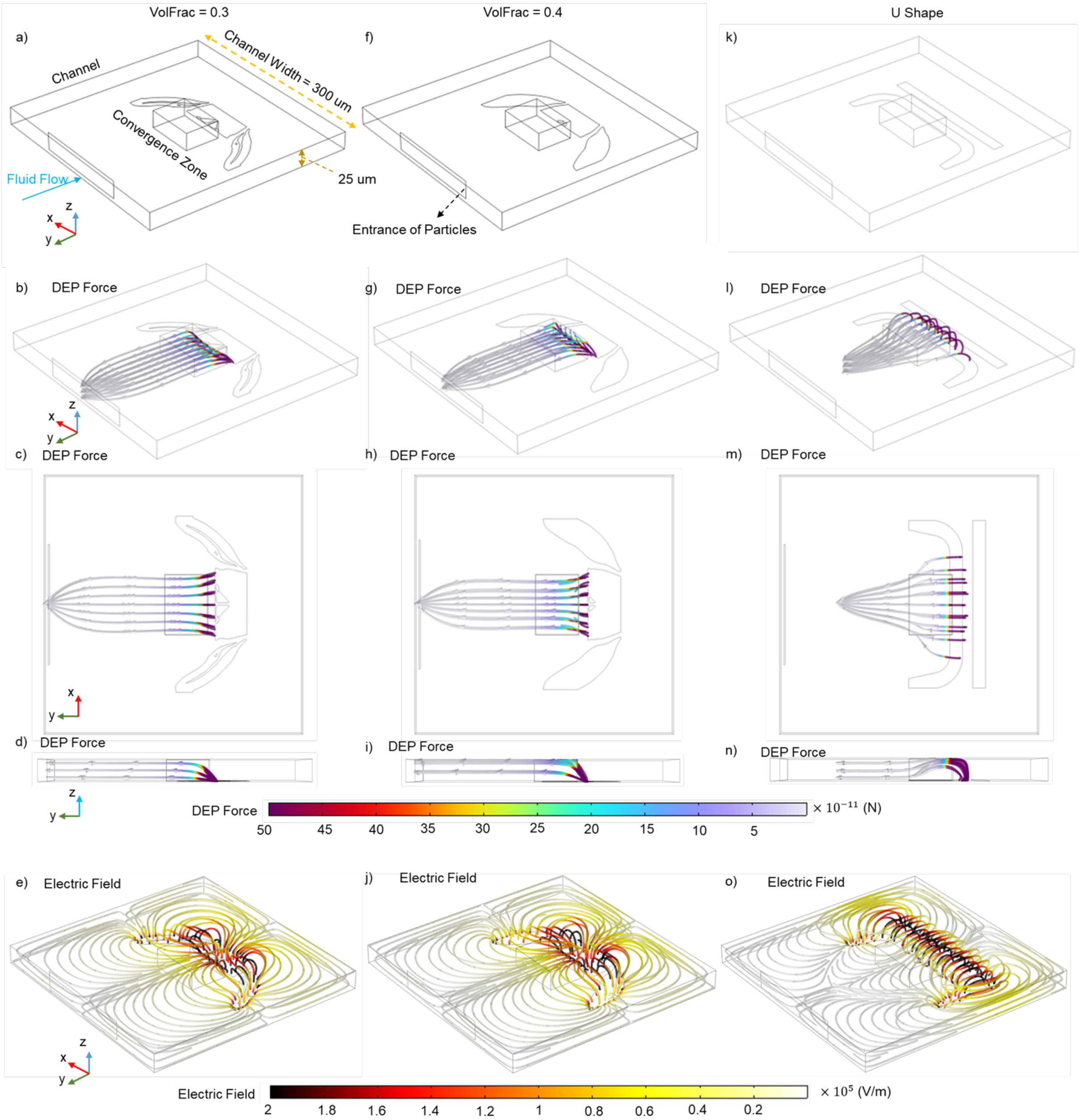

Figure 9: COMSOL 3D simulation results. Stream lines to show the direction and magnitude of the DEP force and the electric field. Colors of stream lines demonstrate the magnitudes referring to color bar.

microfluidic chip devices and more than this channel height, based on plots in Fig. 10-(a & b), the drop in the DEP forces is significant and it may not stop and converge the particles. For the chosen channel height of 25 μm, the DEP forces at the top of the channel for both the center and side points are reported in Table 2. The analysis of Fig. 10) and the data in Table 2 prove the higher efficiency of the optimized design with 0.3 volume fraction in comparison to other designs. The improvement of design with 0.3 volume fraction over the U-shape for the side point at the top of the channel is 2.04 and 1.52 for the y and x DEP forces respectively.

Table 2: Numerical results for the simulation of DEP forces at the top of the channel (height 25 μm) based on Fig. 10

Design	$F_{DEP}X$(N)	Impr	$F_{DEP}Y$(N)	Impr
		Center		
0.3 (Volfrac)	$5.672e^{-12}$	3.18	$1.130e^{-10}$	1.77
0.4 (Volfrac)	$3.039e^{-12}$	1.70	$1.190e^{-10}$	1.89
U-shape	$1.783e^{-12}$	-	$0.627e^{-10}$	-
		Side		
Design	$F_{DEP}X$(N)	Impr	$F_{DEP}Y$(N)	Impr
0.3 (Volfrac)	$6.608e^{-12}$	1.527	$1.347e^{-10}$	2.04
0.4 (Volfrac)	$-3.43e^{-12}$	-0.79	$1.190e^{-10}$	1.808
U-shape	$4.325e^{-12}$	-	$0.658e^{-10}$	-

* Impr = Improvement over U-Shape

7.2. Video Simulations

To better investigate the performance of the optimized designs in terms of trapping the particles in the microfluidic channel of Fig. 9-(a), 3D video simulations are provided by using COMSOL multiphysics. In these simulations, the fluid flow inside the channel is modeled by a laminar flow. The fluid is considered to be water with the speed of 300 μm/sec. Voltages are applied to the electrodes to produce non-uniform electric field and DEP force. The particles are beads (Polystyrene) with 10 μm diameter.

In the video simulations the trapping performances of the optimized designs and the U-shape design can be seen. The entrance of the particles into the channel is considered to be bigger in terms of the width in comparison to the convergence zone which let us see different outcomes based on the initial position of particles. Optimized designs are successfully trapping all the particles coming to the convergence zone. Moreover, they will be pushed to the center of the channel in the direction of x. Other particles that did not enter to the convergence zone, are trapped in other places which are not predetermined. U-shape design also traps all the particles with two major differences in comparison to the optimized designs. The first major difference is that the U-shape design stops the particles very close to the edge of the electrodes where the electric field is maximum. On the other hand, optimized designs stops the particles far from the edge of the electrodes. This makes the optimized designs superior over the U-shape design. However, the advantage of the U-shape design over the optimized design is that it pushes the particles to the bottom of the channel where the DEP force is maximum while the optimized designs push the particles to the top of the channel where the DEP force is minimum.

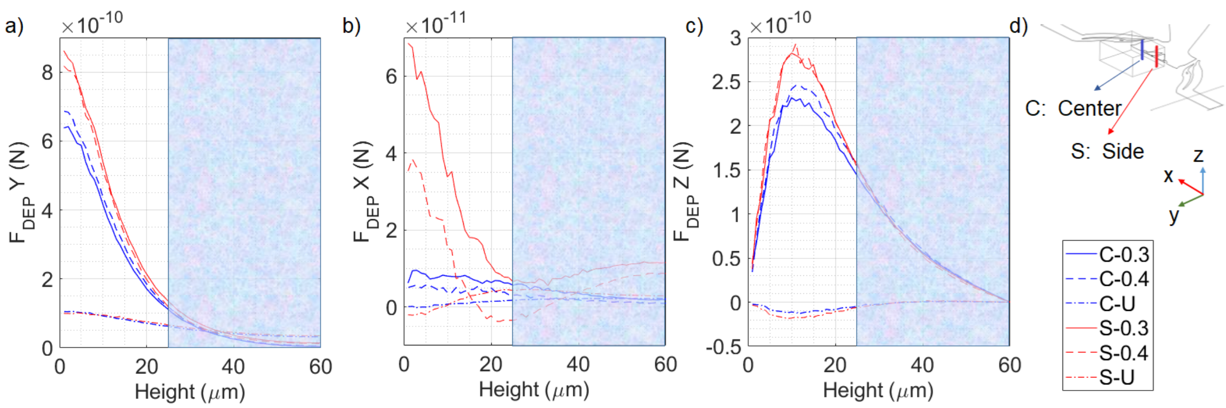

Figure 10: DEP force analysis in the direction of the channel's height. Maximum height of the channel in the experimentation is 25 μm. However, in this figure, the DEP forces are analyzed for the 60 μm channel's height. a) DEP force in the y direction as a function of the channel's height, b) DEP force in the x direction as a function of the channel's height, c) DEP force in the z direction as a function of the channel's height, d) Two possible location for the analysis of the DEP force as a function of channel's height

So far, the performance of the optimized design are analyzed and compared to a U-shape design through 3D simulation by COMSOL Multiphysics software. The next step would be the experimental investigation which requires the fabrication of the proposed designs. This will be the subject of the next section.

7.3. Experimental investigation

In this section, the performances of the optimized designs are investigated through several experimental tests. To do so, first, the proposed designs are fabricated on a fluidic chip, using micro-fabrication technology tools. The substrate of the chip is made of glass and the 200 nm gold electrodes are deposited and patterned by photo-lithography and the channels are made of SU8 resin as can be seen in Fig. 11-(d-e). Through the channel, the fluid with particles can flow while a PDMS layer is used to cover the channel. An experimental bench is set up to flow the fluid and particles inside the channel as it is illustrated in Fig. 11-(a,b,c). The experimental setup and the microfabrication procedure of the fluidic chip are explained more in detail in the appendix.

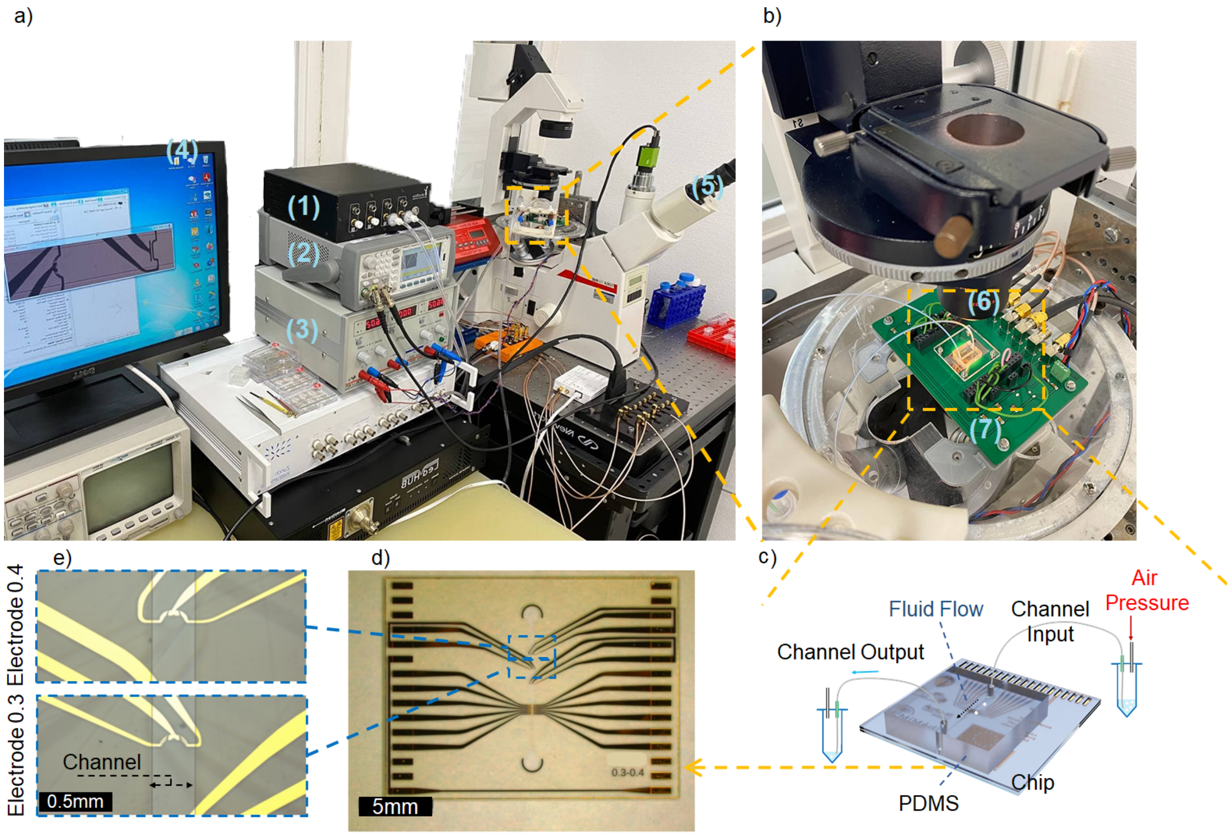

Figure 11: a) Experimental setup, b) Microfluidic chip under the microscope, c) Schematic of the microfluidic chip, d) Fabricated chip in the cleanroom, e) Electrodes magnification under the microscope. Instruments: 1- Air pressure controller, 2- Signal generator, 3- Voltage amplifier, 4- Computer control unit, 5- Microscope, 6- Camera, 7- PCB

The trapping performance of the designs has been investigated on the polystyrene microbeads with 10 μm diameter. The results of the experiments are shown in Fig. 12. The recordings of the experiments are attached as electronic supplementary files. In Fig. 12, several chosen frames for different positions of the particles are illustrated. As it is obvious in these frames, the particle comes from a point that has a distance from the center of the channel (x direction). Then, when it comes close to the electrode, its speed decreases. This is due to the DEP force of the electrode in the y direction. Afterward, the particles shifts slowly to the center of the channel in front of the electrode and rest in that position. This means that the DEP force in the

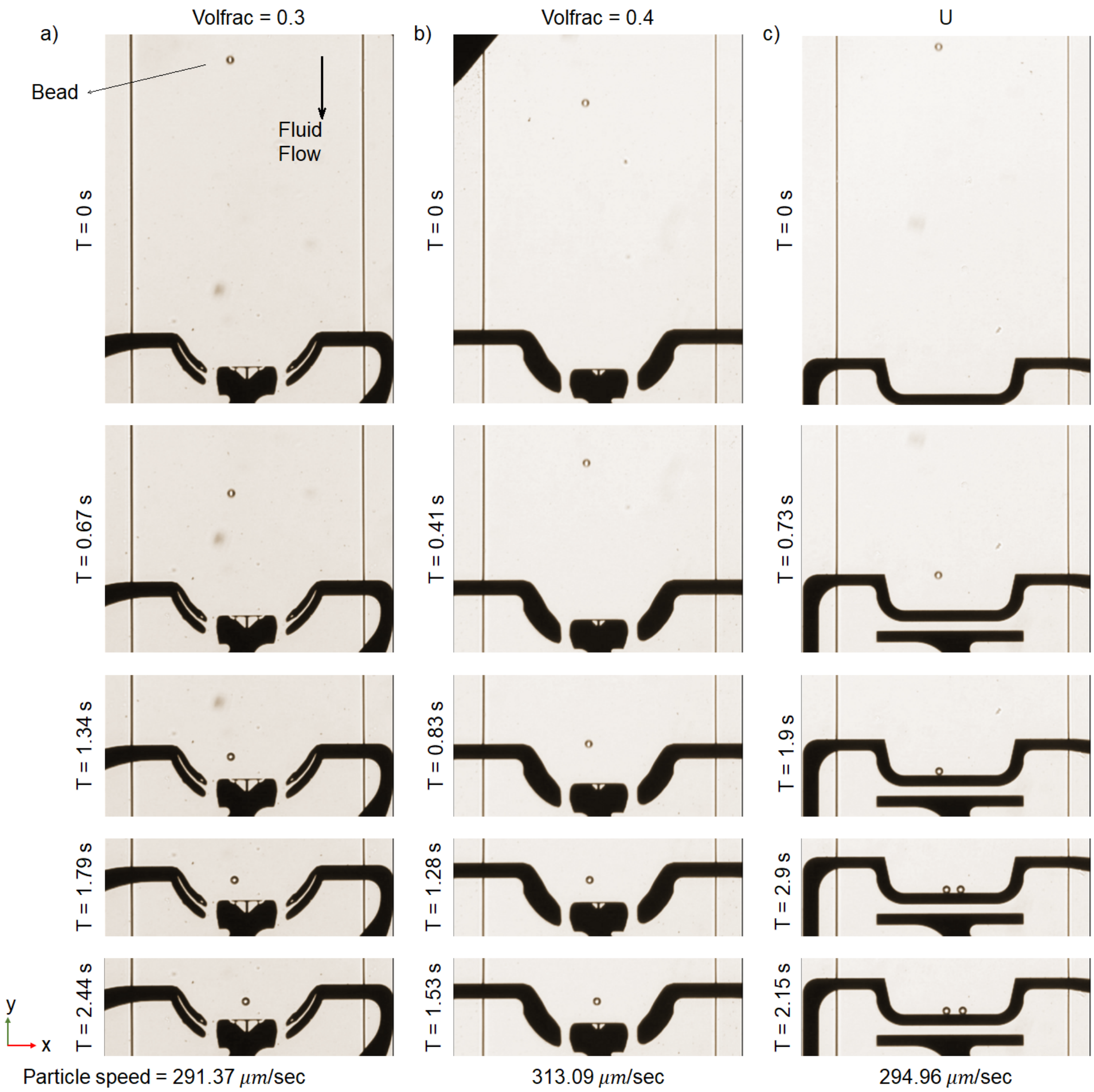

Figure 12: Experimental result for trapping beads. Particles flow inside the channel for three different designs: a) Optimized design with volume fraction 0.3, b) Optimized design with volume fraction 0.4 and c) the U-shape design. T = time (s)

x direction pushes the particle to the center and the combination of the DEP forces in the y and x directions stops the beads at a particular point inside the convergence zone. It can be discovered in Fig. 12 that the electrodes are corroded due to the electrolysis effect and hence the electrode shapes are not completely the same as the optimized ones. This is the inevitable effect of having small features in the electrodes.

In the experiments, we tried different bead speeds to assess the trapping performance of different designs as can be seen in the attached video files. However, to compare the performances in Fig. 12, it is tried to keep the speeds of the beads for different designs close to each other, by controlling the air pressure driving the fluid flow. The performances of the 0.3 and 0.4 designs are similar to each other in terms of trapping the bead. The U-shape design stops the beads on the edge of the electrode where the electric field is maximum. This is in accordance to what was seen in the simulation part. In a sequence of tries with different bead speeds, it was clear that the U-shape design successfully stops the beads against the fluid flow (y direction) on the borders of the electrode. However, the considered U-shape is weak in terms of pushing the particles to the center of the channel in the x direction. This can be due to the fact that the considered U-shape in this paper is a modified (elongated) of the original proposed U-shape [36]. This will be discussed next.

8. Discussion

In the numerical and practical case studies, we tried to prove the efficiency of the developed methodology in terms of defining the direction of the DEP force and modifying the magnitude of the electric field. On the other hand, a more detailed study can be done on the different design and optimization parameters that can affect the obtained results. For example, volume fraction constraint, initially defined potentials, resolution of the mesh, penalty factor in the interpolation function, radius of the filtering method, changing the sharpness and threshold of the projection, weighting factors in the objective function, etc all can affect the result of optimization. Indeed, it may be possible to obtain more efficient layout of the electrodes than what we have reported in this paper. Here, we developed a methodology for optimal design of electrode's shape. Separated studies are needed to investigate the effects of all the aforementioned parameters.

The initially determined potentials can be considered in the optimization problem as well. This needs the definition of additional optimization variables and new sensitivity analysis. This approach will be considered for future studies.

In this paper, a constraint is considered on a sum of the electric field's magnitude in a desired area. Although it was successful in reducing the maximum electric field, The better approach can be the consideration of the local maximum of electric field in the optimization problem which requires new sensitivity analysis and is considered for future studies.

The considered U-shape in this paper has a different geometry from the original U-shape proposed by [36]. The reason for this modification is to keep the surface area and the borders of the domain similar to the design domain of optimization. The chosen design domain provides enough space for the topology optimization to produce efficient results. It is possible to obtain better performance from U-shape by changing its geometry. On the other hand, this is also true for the results obtained by topology optimization. The idea of comparison with the U-shape is to challenge the proposed methodology against an existing layout. Otherwise, finding the best results by changing the parameters of optimizations is up to readers as explained before.

The limits of the developed methodology mainly lie in the fabrication process. The small features that can appear in the optimized electrode design are complicated to fabricate. Moreover, those small features can result in the electrolysis phenomenon when applying the voltage to the electrode that erodes the electrode. The fabrication constraints can be considered in the topology optimization method in future studies. To avoid the small feature in the obtained design one can increase the filter radius as an optimization parameter.

The size of the beads in the experiments is chosen to be 10 μm which is close to the size of the biological cells including lymphocytes in the medical therapy devices. We demonstrated that for this size of the beads and the channel height of 25 μm, the DEP force is strong enough to stop the beads. For higher channel height, the convergence efficiency of the electrodes will drop due to the low magnitude of the DEP force. This can be ameliorated by considering the electrodes on the top and bottom of the channel. Consequently, the generality of the proposed approach remains intact.

9. Conclusion

In this paper, a detailed FEM is employed to model the DEP force and electric field induced by electrodes. Based on this FEM, a general optimization problem is formulated to determine the direction of the DEP force, maximize its magnitude and minimize the magnitude of the electric field. SIMP topology optimization approach is implemented by deriving the explicit formulation of the sensitivity analysis to perform a gradient-based optimization. The performance of the methodology is assessed in several numerical case studies. It has been demonstrated that the developed optimization methodology can optimize the shape of the electrode in order to determine the direction of the DEP force and minimize the magnitude of the electric field. After numerical investigation, the performance of the methodology is demonstrated in a real practical application. It has been demonstrated by 3D COMSOL simulation that optimized 2D electrode is efficient enough for a limited height of the channel. This is later approved by experimental investigation and the efficiency of the optimized electrode is demonstrated in comparison to an electrode design similar to the layout existing the literature.

The future perspective of the research can be the extension of the FEM approach from 2D to 3D. In this way, the behavior of the DEP force in the direction of the channel's height can be taken into consideration in the optimization problem. Moreover, designing the 3D electrodes on all surfaces of the channel instead of considering them just at the bottom of the channel can be done with the help of 3D modeling and optimization while doing so intuitively is considerably challenging.

Conflicts of interest

There are no conflicts to declare.

Acknowledgements

This work was supported in part by the EIPHI Graduate School under Contract ANR- 17-EURE-0002, in part by the MiMedi project funded by BPI France under Grant DOS0060162/00 and by the European Union through the European Regional Development Fund of the Region Bourgogne-Franche-Comté under Grant FC0013440 and in part by the french RENATECH network and its FEMTO-ST technological facility.

Appendix

Reminder of Finite element method

In this section, we will remind the important part of the finite element method which is necessary for modeling and sensitivity analysis in this paper.

The goal here is to calculate the electric field and its gradient based on the natural coordinates of the square parent element. To begin with, the gradient interpolation matrix mentioned in equation (7), can be expressed as

$$B = \begin{bmatrix} B_\xi \\ B_\eta \end{bmatrix} = \begin{bmatrix} b_{1,1}(\xi,\eta) & b_{1,2}(\xi,\eta) & \dots & b_{1,8}(\xi,\eta) \\ b_{2,1}(\xi,\eta) & b_{2,2}(\xi,\eta) & \dots & b_{2,8}(\xi,\eta) \end{bmatrix} \tag{40}$$

In this equation, ξ and η are the natural coordinates as it has been shown in Fig. 3-(d). $b_{i,j}(\xi,\eta)$ in equation (40) is the derivation of the shape functions with respect to the natural coordinates. The shape functions of the 8 node rectangular element and their derivatives can be found in [45].

The calculation of gradient interpolation matrix is now used to calculate the elemental dielectric matrix.

$$k = \int_{\Omega^e} B^T \varepsilon B d\Omega = \int_{-1}^{+1} \int_{-1}^{+1} B^T \varepsilon B \left|\bar{J}\right| d\xi d\eta \tag{41}$$

in which $\left|\bar{J}\right|$ is the determinant of the Jacobean matrix to map the coordinate system from global coordinate to the natural coordinate [42]. The integration over each element can be done using the numerical Gauss quadrature method [42]. Moreover, the calculation of gradient interpolation matrix is used in calculation of the decomposition of electric field as it is mentioned in equation (11). However, The gradient interpolation matrix (B) is right now based on the natural coordinate system while we need the gradient interpolation matrix in the global coordinates. Since we are using the rectangular element to discretize the design domain which is a particular form of quadrilateral elements, transferring from natural coordinates to global coordinates is straightforward [42],

$$\begin{aligned} \frac{\partial}{\partial x} &= \frac{\partial}{\partial \xi}\frac{\partial \xi}{\partial x} = \frac{1}{le}\frac{\partial}{\partial \xi} \\ \frac{\partial}{\partial y} &= \frac{\partial}{\partial \eta}\frac{\partial \eta}{\partial x} = \frac{1}{we}\frac{\partial}{\partial \eta} \end{aligned} \tag{42}$$

Therefore, the vector of electric field for each element can be calculated as

$$\begin{bmatrix} E_x \\ E_y \end{bmatrix} = \begin{bmatrix} \frac{1}{le} & 0 \\ 0 & \frac{1}{we} \end{bmatrix} \begin{bmatrix} B_\xi \\ B_\eta \end{bmatrix} \begin{bmatrix} \phi_1 \\ \phi_2 \\ \phi_3 \\ \phi_4 \\ \phi_5 \\ \phi_6 \\ \phi_7 \\ \phi_8 \end{bmatrix} \tag{43}$$

and gradient interpolation matrices can be expressed as

$$B_x = \frac{1}{le} B_\xi, \quad B_y = \frac{1}{we} B_\eta \tag{44}$$

The crucial part in our finite element modeling and calculation of DEP force is the Gradient of the electric field. Using the natural coordinates, the derivatives if the electric fields can be calculated as,

$$\begin{aligned} \frac{\partial}{\partial y} E_x &= \frac{\partial}{\partial y} B_x \phi = \frac{1}{we} \frac{\partial}{\partial \eta} B_x \phi = B_{x,y} \phi \\ \frac{\partial}{\partial y} E_y &= \frac{\partial}{\partial y} B_y \phi = \frac{1}{we} \frac{\partial}{\partial \eta} B_y \phi = B_{y,y} \phi \\ \frac{\partial}{\partial x} E_x &= \frac{\partial}{\partial x} B_x \phi = \frac{1}{le} \frac{\partial}{\partial \xi} B_x \phi = B_{x,x} \phi \\ \frac{\partial}{\partial x} E_y &= \frac{\partial}{\partial x} B_y \phi = \frac{1}{le} \frac{\partial}{\partial \xi} B_y \phi = B_{y,x} \phi \end{aligned} \tag{45}$$

These relations, makes the calculation of the gradient of electrical field in equation (13) straightforward.

Validation of the developed FEM

To validate the developed FEM in this paper, the results obtained by MATLAB are compared to the ones from COMSOL multiphysics. In Fig. 13, the potential field, electric field and the DEP force for the two optimized designs which are calculated by MATLAB are compared with COMSOL FEM results. In panels (d) and (e), the color spectrum demonstrates the magnitude of electric field. In panels (g) and (h) of Fig. 13 the color spectrum shows the magnitude of the DEP force and arrows represent the direction of the DEP force. The numerical values of the two methods are calculated on a particular line which is chosen randomly and are plotted in panels (c), (f) and (i) of Fig. 13.

The agreement between the developed FEM in MATLAB and the FEM in COMSOL for potential and electric field is quite satisfying. For the DEP force, MATLAB demonstrates a jump in the magnitude of the DEP force at the borders of the electrode. The reason is that, at the borders of the electrodes there is a sudden change in the potential and with a two times derivation it manifests as a high value. This jump is not seen in the COMSOL software due to change in the mesh size at the borders of the electrode. In fact, COMSOL is using a mesh with variable size triangular elements to discretize the design domain and it captures the edge more precisely while in MATLAB we are using constant size rectangular elements and there are huge changes in the potential values in one element which manifest high values in the second derivation with respect to potential.

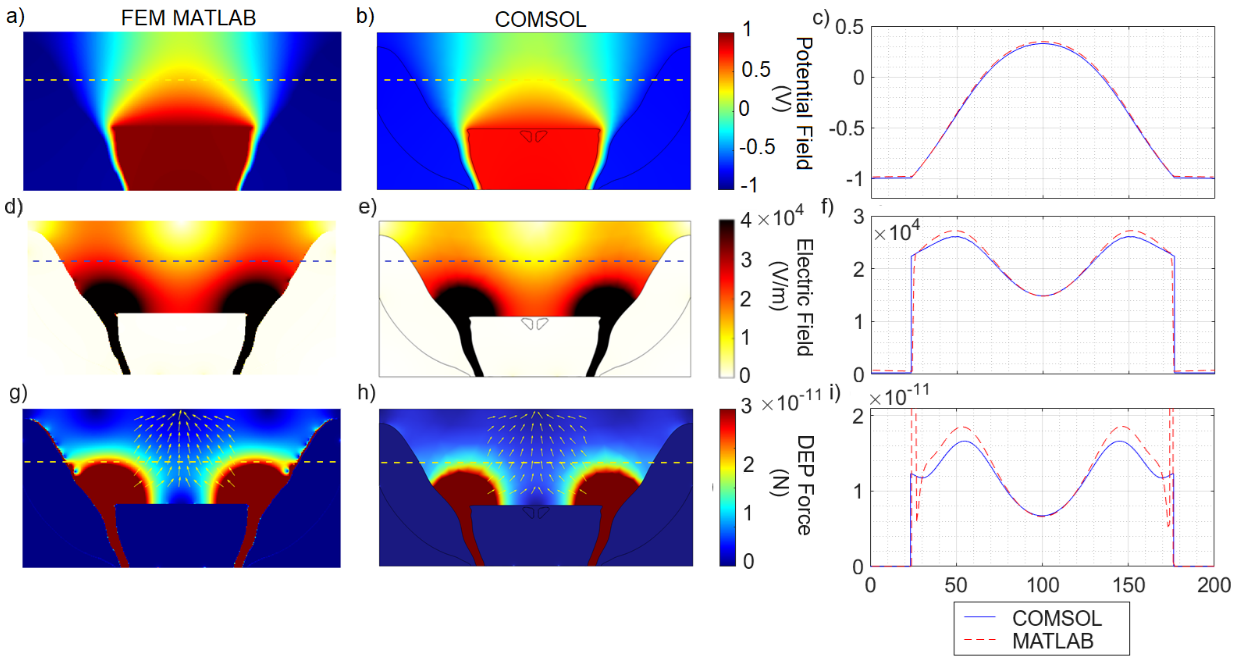

Figure 13: Validation of developed FEM for potential and electric fields and DEP force. Arrows represents the normalized DEP force. a), d) and g), FEM developed in MATLAB. b), e) and h), COMSOL simulation. c), f), i) Numerical values are reported over the dash lines.

Validation of sensitivity analysis by CDM

In Central Difference Method (CDM), the derivative of objective function with respect to the optimization variables can be calculated using the following equation [48],

$$\frac{d\mathbb{J}(\gamma)}{d\gamma_e} = \frac{\mathbb{J}(\gamma + \mathit{\Delta} h) - \mathbb{J}(\gamma - \mathit{\Delta} h)}{2\mathit{\Delta} h} \tag{46}$$

in which $\mathit{\Delta} h$ is a vector containing zeros for all elements except the one corresponds to element $\{e\}$. With CDM it is possible to calculate the sensitivities. However, to calculate the sensitivity of each element, the global equilibrium finite element equation (10) should be solved two times. This makes the calculation of sensitivities by CDM extremely time consuming. That is why to verify the proposed sensitivity analysis, a coarse mesh is considered (10×20 elements). The result of sensitivities with two different methods are reported in Fig. 14 for $\mathit{\Delta} h = 1e^{-6}$. These sensitivities are related to the case study which is illustrated in Fig. 5. The plots show an excellent agreement between two methods and verify the accuracy of the proposed sensitivity analysis.

Fabrication of Fluidic Chip

The microfluidic chips are manufactured by the flowchart adapted from [57] which follows a simple known manufacturing processes. First, 200nm of gold is deposited on 20nm of titanium (adhesion layer) by evaporation (*Plassys, EVAP MEB600*) on a borosilicate (BF33) wafer as a substrate. To create the microfluidic channel, a negative photosensitive resin (*SU-8 3500*) is spin-coated with chosen spin-coating parameters to reach the desired thickness of the resin i.e. the desired height of the fluidic channel. A mask is laser-written (*Heidelberg, Laser Lithography System MLA150*) and used for UV exposure to polymerize the walls of the fluidic channels (*EVG, Aligner DUV* with a specific SU-8 filter, $E = 300mJ$), quickly followed by a post-expose bake. Then, the wafer is put in a *PGMEA* developer bath for few minutes with strong agitation to discover

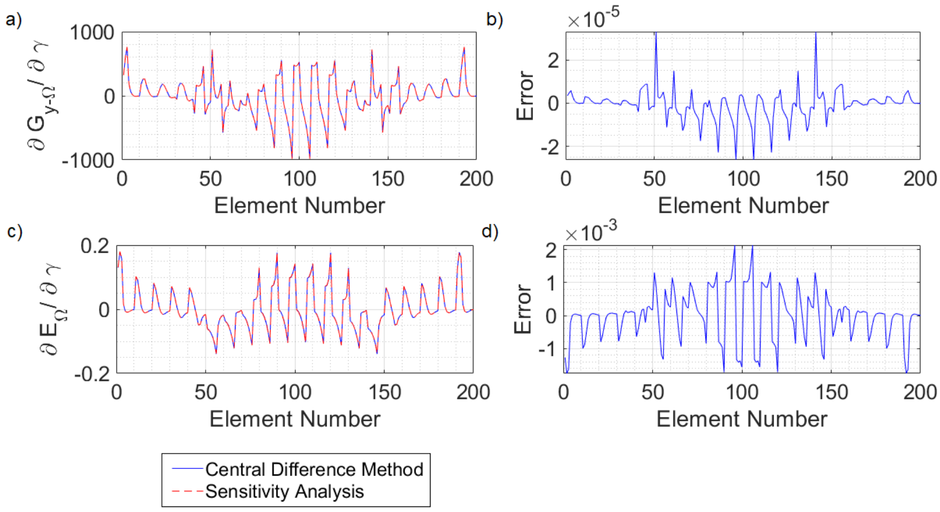

Figure 14: Validation of sensitivity analysis. a,b) Sensitivities calculated by CDM and explicit formulations b,d) Absolute error between two methods

the pattern of the fluidic walls, permanently fixed at the end by a hard-bake, preceded by a short plasma O2 etching to ensure the cleanliness of the substrate. The wafer is finally cut into the final different chips (*DISCO, Dicing Saw DAD 3350*) as it is illustrated in Fig. 11-(d & e). All of the electrode designs are fabricated on one chip to ensure the same particle speed in all the experiments. To seal each microfluidic chip, a PDMS cover is used, consisting simply a cast PDMS layer of about half a cm thick, cut at the right dimensions and punched for the fluidic inlet tubing connection. The PDMS is simply pressed on top of the chip and kept in place by a dedicated screwed plexiglass holder.

Experimental Setup

To apply a specific voltage to each electrode of the microfluidic chip, a homemade PCB is used to plug and hold the chip (Fig. 11-(b)) and connect its electronic pads to the desired signals. A NI card (PCI-6733) is used to control the voltage amplitude coming from the computer DC voltage to the NI interface card (BNC-2110). Another homemade PCB is used to multiply the DC voltage by a shared AC signal (Waveform Generator *KEYSIGHT 33500B Series*) at $100kHz$, whose amplitude is set to $6V$. The generated AC signal is then sent to the chip. The experiments are monitored through a camera (*JAI, GO-5000C*) placed on the microscope (*LEICA DM IRBE*, ×10 magnification). As the homemade PCB holding the chip is fixed on a XYZ-table under the microscope it is possible to visualize the fluidic channel and adjust the monitoring location as we are controlling the signals and the fluid flow.

The fluidic system is described as follows. An air pressure controller (*Elveflow, OB1 Pressure Controller*) is used to set a specific air pressure in a sealed fluidic tank (*Eppendorf Tube* $2ml$) containing around $100\mu l$ of the solution with the beads. The fluidic microtubing (*Darwin Microfluidic PTFE teflon capillary microtube* $diameter_{ext} = 760\mu m, diameter_{int} = 300\mu m$) inside the solution is connecting the sealed tank to the chip through the punched PDMS cover. The same system is used for the fluidic outlet with another tank. Applying stronger air pressure to the inlet allows the displacement of the fluid inside the microfluidic chip as a laminar flow. As air bubbles can escape through the porous PDMS cover, the fluidic resistances of the whole fluidic system are almost constant and the fluid flow remains quite stable with a constant target pressure. Changing the air pressure changes directly the fluid speed in a few milliseconds. Images are post-treated to find the speed of the particles.

The medium electric properties for the beads: the relative permittivity is $\varepsilon_{rm} = 78$ and the electric conductivity is $\sigma_m = 0.16\ S/m$. To reach this conductivity value, the beads were suspended in a PBS (Phosphate Buffered Saline) medium diluted ten times in deionized (DI) water. $0,1\%$ of *Tween20* is also added to keep the beads from sticking to the substrate and to each other.

References

[1] H. Pohl, H. Pohl, Dielectrophoresis: the behavior of neutral matter in nonuniform electric fields. 1978, Barsotti, R., Vahey, M., Wartena, R., Chiang, Y.-M., Voldman, J., Stellacci, F. Small 3 (2007) 488–499.

[2] V. Gauthier, A. Bolopion, M. Gauthier, Analytical formulation of the electric field induced by electrode arrays: Towards automated dielectrophoretic cell sorting, Micromachines 8 (8) (2017) 253.

[3] A. Lefevre, V. Gauthier, M. Gauthier, A. Bolopion, Closed-loop control of particles based on dielectrophoretic actuation, IEEE/ASME Transactions on Mechatronics (2022).

[4] T. Kodama, T. Osaki, R. Kawano, K. Kamiya, N. Miki, S. Takeuchi, Round-tip dielectrophoresis-based tweezers for single micro-object manipulation, Biosensors and Bioelectronics 47 (2013) 206–212.

[5] J. Myung, S. Hong, Microfluidic devices to enrich and isolate circulating tumor cells, Lab on a Chip 15 (24) (2015) 4500–4511.

[6] O. O. Saeed, R. Li, Y. Deng, et al., Microfluidic approaches for cancer cell separation, Journal of Biomedical Science and Engineering 7 (12) (2014) 1005.

[7] A. Alazzam, B. Mathew, F. Alhammadi, Novel microfluidic device for the continuous separation of cancer cells using dielectrophoresis, Journal of separation science 40 (5) (2017) 1193–1200.

[8] H. Li, R. Bashir, Dielectrophoretic separation and manipulation of live and heat-treated cells of listeria on microfabricated devices with interdigitated electrodes, Sensors and actuators B: chemical 86 (2-3) (2002) 215–221.

[9] N. Demierre, T. Braschler, R. Muller, P. Renaud, Focusing and continuous separation of cells in a microfluidic device using lateral dielectrophoresis, Sensors and Actuators B: Chemical 132 (2) (2008) 388–396.

[10] L. D'Amico, N. Ajami, J. Adachi, P. Gascoyne, J. Petrosino, Isolation and concentration of bacteria from blood using microfluidic membraneless dialysis and dielectrophoresis, Lab on a Chip 17 (7) (2017) 1340–1348.

[11] P. R. Gascoyne, J. V. Vykoukal, Dielectrophoresis-based sample handling in general-purpose programmable diagnostic instruments, Proceedings of the IEEE 92 (1) (2004) 22–42.

[12] X. Hu, P. H. Bessette, J. Qian, C. D. Meinhart, P. S. Daugherty, H. T. Soh, Marker-specific sorting of rare cells using dielectrophoresis, Proceedings of the national academy of sciences 102 (44) (2005) 15757–15761.

[13] K. Khoshmanesh, C. Zhang, F. J. Tovar-Lopez, S. Nahavandi, S. Baratchi, K. Kalantar-zadeh, A. Mitchell, Dielectrophoretic manipulation and separation of microparticles using curved microelectrodes, Electrophoresis 30 (21) (2009) 3707–3717.

[14] H. Zhang, H. Chang, P. Neuzil, Dep-on-a-chip: Dielectrophoresis applied to microfluidic platforms, Micromachines 10 (6) (2019) 423.

[15] T. Z. Jubery, P. Dutta, A new design for efficient dielectrophoretic separation of cells in a microdevice, Electrophoresis 34 (5) (2013) 643–650.

[16] H. Sadeghian, Y. Hojjat, M. Soleimani, Interdigitated electrode design and optimization for dielectrophoresis cell separation actuators, Journal of Electrostatics 86 (2017) 41–49.

[17] S. Kinio, J. K. Mills, Design of electrode topologies for dielectrophoresis through the use of genetic optimization with comsol multiphysics, in: 2015 IEEE International Conference on Mechatronics and Automation (ICMA), IEEE, 2015, pp. 1019–1024.

[18] S. Kinio, J. K. Mills, Design of optimal electrode geometries for dielectrophoresis using fitness based on simplified particle trajectories, Biomedical microdevices 18 (4) (2016) 1–15.

[19] C.-H. Han, H. W. Ha, J. Jang, Two-dimensional computational method for generating planar electrode patterns with enhanced volumetric electric fields and its application to continuous dielectrophoretic bacterial capture, Lab on a Chip 19 (10) (2019) 1772–1782.

[20] G. H. Yoon, J. Park, Topological design of electrode shapes for dielectrophoresis based devices, Journal of Electrostatics 68 (6) (2010) 475–486.

[21] T. B. Napotnik, T. Polajžer, D. Miklavčič, Cell death due to electroporation–a review, Bioelectrochemistry 141 (2021) 107871.

[22] M. P. Bendsoe, N. Kikuchi, Generating optimal topologies in structural design using a homogenization method, Computer Methods in Applied Mechanics and Engineering (1988).

[23] H. Zhang, Y. Wang, Z. Kang, Topology optimization for concurrent design of layer-wise graded lattice materials and structures, International Journal of Engineering Science 138 (2019) 26–49.

[24] M. P. Bendsoe, O. Sigmund, Topology optimization: theory, methods, and applications, Springer Science & Business Media, 2003.

[25] T. Dbouk, A review about the engineering design of optimal heat transfer systems using topology optimization, Applied Thermal Engineering 112 (2017) 841–854.

[26] Y. Chen, S. Zhou, Q. Li, Multiobjective topology optimization for finite periodic structures, Computers & Structures 88 (11-12) (2010) 806–811.

[27] J. Alexandersen, C. S. Andreasen, A review of topology optimisation for fluid-based problems, Fluids 5 (1) (2020) 29.

[28] K. A. James, G. J. Kennedy, J. R. Martins, Concurrent aerostructural topology optimization of a wing box, Computers & Structures 134 (2014) 1–17.

[29] R. E. Christiansen, O. Sigmund, Compact 200 line matlab code for inverse design in photonics by topology optimization: tutorial, JOSA B 38 (2) (2021) 510–520.

[30] A. Homayouni-Amlashi, A. M. Ousaid, M. Rakotondrabe, Multi directional piezoelectric plate energy harvesters designed by topology optimization algorithm, IEEE Robotics and Automation Letters (2019).

[31] A. Homayouni-Amlashi, A. Mohand-Ousaid, M. Rakotondrabe, Topology optimization of 2dof piezoelectric plate energy harvester under external in-plane force, Journal of Micro-Bio Robotics (2020) 1–13.

[32] A. Homayouni-Amlashi, T. Schlinquer, A. Mohand-Ousaid, M. Rakotondrabe, 2d topology optimization matlab codes for piezoelectric actuators and energy harvesters, Structural and Multidisciplinary Optimization 63 (2) (2021) 983–1014.

[33] Y. Li, L. Liu, S. Yang, Z. Ren, Y. Ma, A multi-objective topology optimization methodology and its application to electromagnetic actuator designs, IEEE Transactions on Magnetics 56 (2) (2020) 1–4.
[34] K. Svanberg, The method of moving asymptotes—a new method for structural optimization, International journal for numerical methods in engineering 24 (2) (1987) 359–373.
[35] K. Svanberg, Mma and gcmma-two methods for nonlinear optimization, vol 1 (2007) 1–15.
[36] M. Punjiya, H. R. Nejad, J. Mathews, M. Levin, S. Sonkusale, A flow through device for simultaneous dielectrophoretic cell trapping and ac electroporation, Scientific reports 9 (1) (2019) 1–11.
[37] T. B. Jones, Fundamentals, Cambridge University Press, 1995, p. 5–33.
[38] X. Wang, X.-B. Wang, P. R. Gascoyne, General expressions for dielectrophoretic force and electrorotational torque derived using the maxwell stress tensor method, Journal of electrostatics 39 (4) (1997) 277–295.
[39] R. D. Cook, et al., Concepts and applications of finite element analysis, John wiley & sons, 2007.
[40] J.-H. Kim, S.-H. Kang, S. Cho, Shape design optimization of interdigitated electrodes for maximal electro-adhesion forces, Structural and Multidisciplinary Optimization 61 (2020) 1843–1855.
[41] B. Zheng, C.-J. Chang, H. C. Gea, Topology optimization of energy harvesting devices using piezoelectric materials, Structural and Multidisciplinary Optimization 38 (1) (2009) 17–23.
[42] D. V. Hutton, J. Wu, Fundamentals of finite element analysis, Vol. 1, McGraw-hill New York, 2004.
[43] A. C. Polycarpou, Introduction to the finite element method in electromagnetics, Synthesis Lectures on Computational Electromagnetics 1 (1) (2005) 1–126.
[44] R. Bargallo, Finite elements for electrical engineering, Universitat Politecnica De Catalunya (2006).
[45] D. L. Logan, A first course in the finite element method, Cengage Learning, 2016.
[46] K. Maute, O. Sigmund, Topology optimization approaches: A comparative review, Structural and Multidisciplinary Optimization 6 (2013) 1031–1055.
[47] E. Andreassen, A. Clausen, M. Schevenels, B. S. Lazarov, O. Sigmund, Efficient topology optimization in matlab using 88 lines of code, Structural and Multidisciplinary Optimization 43 (1) (2011) 1–16.
[48] R. Alberdi, G. Zhang, L. Li, K. Khandelwal, A unified framework for nonlinear path-dependent sensitivity analysis in topology optimization, International Journal for Numerical Methods in Engineering 115 (1) (2018) 1–56.
[49] J. Jung, J. Hyun, S. Goo, S. Wang, An efficient design sensitivity analysis using element energies for topology optimization of a frequency response problem, Computer Methods in Applied Mechanics and Engineering 296 (2015) 196–210.
[50] S. Cho, J.-Y. Choi, Efficient topology optimization of thermo-elasticity problems using coupled field adjoint sensitivity analysis method, Finite Elements in Analysis and Design 41 (15) (2005) 1481–1495.
[51] F. Wang, B. S. Lazarov, O. Sigmund, On projection methods, convergence and robust formulations in topology optimization, Structural and multidisciplinary optimization 43 (6) (2011) 767–784.
[52] F. Ferrari, O. Sigmund, A new generation 99 line matlab code for compliance topology optimization and its extension to 3d, Structural and Multidisciplinary Optimization 62 (4) (2020) 2211–2228.
[53] T. Schlinquer, A. Mohand-Ousaid, M. Rakotondrabe, Displacement amplifier mechanism for piezoelectric actuators design using simp topology optimization approach, in: IEEE ICRA, 2018, pp. 1–7.
[54] S. H. Kim, M. Antfolk, M. Kobayashi, S. Kaneda, T. Laurell, T. Fujii, Highly efficient single cell arraying by integrating acoustophoretic cell pre-concentration and dielectrophoretic cell trapping, Lab on a Chip 15 (22) (2015) 4356–4363.
[55] J. Yao, G. Zhu, T. Zhao, M. Takei, Microfluidic device embedding electrodes for dielectrophoretic manipulation of cells-a review, Electrophoresis 40 (8) (2019) 1166–1177.
[56] E. Sollier, D. E. Go, J. Che, D. R. Gossett, S. O'Byrne, W. M. Weaver, N. Kummer, M. Rettig, J. Goldman, N. Nickols, et al., Size-selective collection of circulating tumor cells using vortex technology, Lab on a Chip 14 (1) (2014) 63–77.
[57] B. Brazey, J. Cottet, A. Bolopion, H. Van Lintel, P. Renaud, M. Gauthier, Impedance-based real-time position sensor for lab-on-a-chip devices, Lab on a Chip 18 (5) (2018) 818–831.